VIRGINIA POLYTECHNIC INSTITUTE
AND STATE UNIVERSITY

The Charles E. Via, Jr. Department
of Civil and Environmental Engineering
Blacksburg, VA 24061

Structural Engineering and Materials

FLEXURAL STRENGTH OF EXTERIOR METAL BUILDING WALL ASSEMBLIES WITH RIGID INSULATION

by
Tian Gao
Graduate Research Assistant

Cristopher D. Moen, Ph.D., P.E.
Principal Investigator

Submitted to the:

Metal Building Manufacturers Association
1300 Sumner Ave
Cleveland, OH 44115-2851

Report No. CE/VPI-ST-11/01

August 2011

Table of Contents

1. Introduction

The critical design case for cold-formed steel wall girts in metal building is suction caused by wind. This wind loading places a girt's unbraced flange in compression, resulting in restrained lateral-torsional buckling. Rotational restraint provided to the girt by through-fastened metal panels is complicated to predict, and therefore through-fastened girt flexural capacity is approximated with experimentally derived strength reduction factors, i.e., R-factors, as described in AISI S100-07 D6.1.1 (AISI 2007).

Recent emphasis on energy efficiency from the U.S. Department of Energy is resulting in more stringent energy efficiency standards for buildings. These new standards have encouraged the metal building industry to explore the improved continuous thermal barrier provided by rigid board insulation. However, the influence of the rigid board thickness and material properties on restrained girt lateral-torsional buckling, i.e., the R-factor, has not investigated.

The goal of this research study is to observe and quantify the influence of rigid board insulation on through-fastened girt capacity. Rotational restraint tests are performed to study local rotational stiffness at the flange-insulation contact point. Vacuum box tests on through-fastened wall systems are conducted to explore the effect of insulation thickness on the R-factor. The results will be used to support new code language in AISI S100-07 D6.1 that accommodate capacity prediction of metal building wall systems with rigid board insulation.

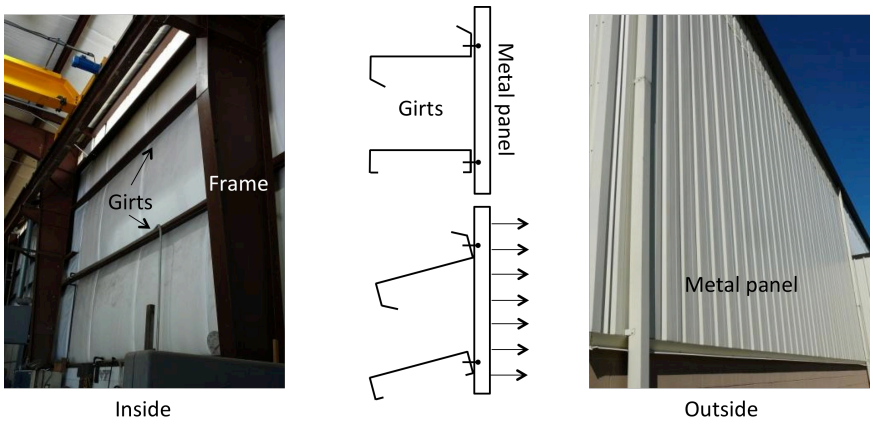

Figure 1: Wind suction on a metal building wall system

A metal building wall system consists of girts and metal panels as shown in Figure 1. The girts typically have a Zee or Cee cross-section, with one flange through-fastened to the panel. Wind suction pulls the panel away from the building, placing the unbraced flange in compression. In design, the tension flange is assumed fully restrained in lateral translation and partially restrained in rotation by the panel (AISI 2007). The girt cross-section rotates around the flange-web intersection in a Zee section and around the flange-stiffening lip intersection in a Cee section due to the lateral-torsional buckling (LaBoube 1986). The wall girt capacity is a function of panel-to-girt rotational restraint, K_o, which can be evaluated by a rotational restraint test, historically referred to as an F-test (LaBoube 1986; Schafer et al. 2007).

2. Panel-Girt Rotational Restraint

2.1 Experiments

Experiments were performed to quantify the rotational restraint provided by through fastened wall panels to girts with Cee and Zee cross-sections. Note that this section focuses on panel-girt interaction *without insulation*. The tests were conducted at Johns Hopkins University with the test procedure motivated by Schafer et al. (2007). Each specimen is an assembly of a 5 ft long Cee or Zee section cold-formed steel girt and two 0.018 in. thick 3 ft x 6 ft panels. The two panels are joined using #12 fasteners at the edges to form a 6 ft x 6 ft panel. The girt flange is through-fastened to the panel with #12-14 self drilling screws every 12 in. directly next to the rib. The panel cross-section is shown in Figure 2.

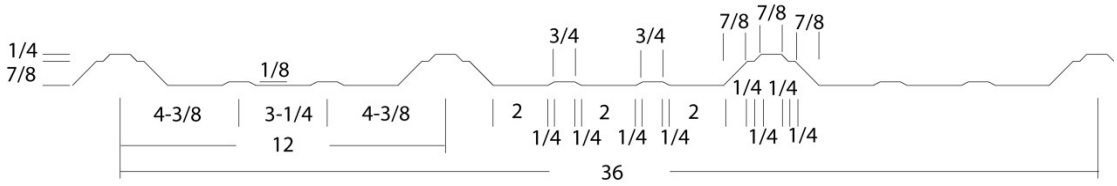

Figure 2: Panel cross-section (in.)

Specimen names and girts details are provided in Table 1. The notation *C*, *B* and *h* are illustrated in Figure 3. The thickness, *t*, represents the bare metal thickness.

Table 1: The specimen names and girts details

Specimen name	Member Profile	Member depth, *h* (in.)	Average *B* (in.)	Average *C* (in.)	Thickness bare, *t* (in.)
Z8-1	Z	8	---	1.13	0.102
Z8-2	Z	8	---	1.34	0.102
Z10-1	Z	10	---	1.31	0.106
Z10-2	Z	10	---	1.41	0.106
C8-1	C	8	1.47	1.15	0.103
C8-2	C	8	1.15	1.18	0.103
C250-1	C	10	1.61	1.47	0.105
C150-1	C	6	0.95	1.05	0.069

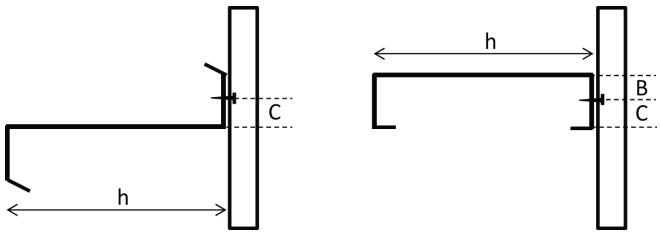

Figure 3: *h*: the member depth. *C*: the distance between the screw and corner of the web and flange in Zee section (corner of the lip and flange in Cee section). *B*: the distance between the screw and corner of the web and flange in a Cee section

The test setup is illustrated in Figure 4. The base of the specimen is clamped between 6 x 4 x 0.31 in. angles. The angles have pre-drilled holes every 5.76 in., and are through-fastened and clamped with 5/8 in. diameter structural bolts. Plaster casts 6 in. high are placed between the angles and the ribs to prevent crushing of the panel. A vertical load, Q, is applied at the free member flange with a 22 kip MTS hydraulic actuator. The actuator is free to move horizontally on frictionless rollers to maintain a vertical loading. The member-panel connection point is 45 in. from the top of the clamping angle. A pair of position transducers is used to measure the horizontal deflection, H, of the panel. The transducers are set 5 in. below the connection to avoid the effect of panel local deformation. The vertical displacement, V, and the loading, Q, are recorded by an LVDT and load cell inside the actuator.

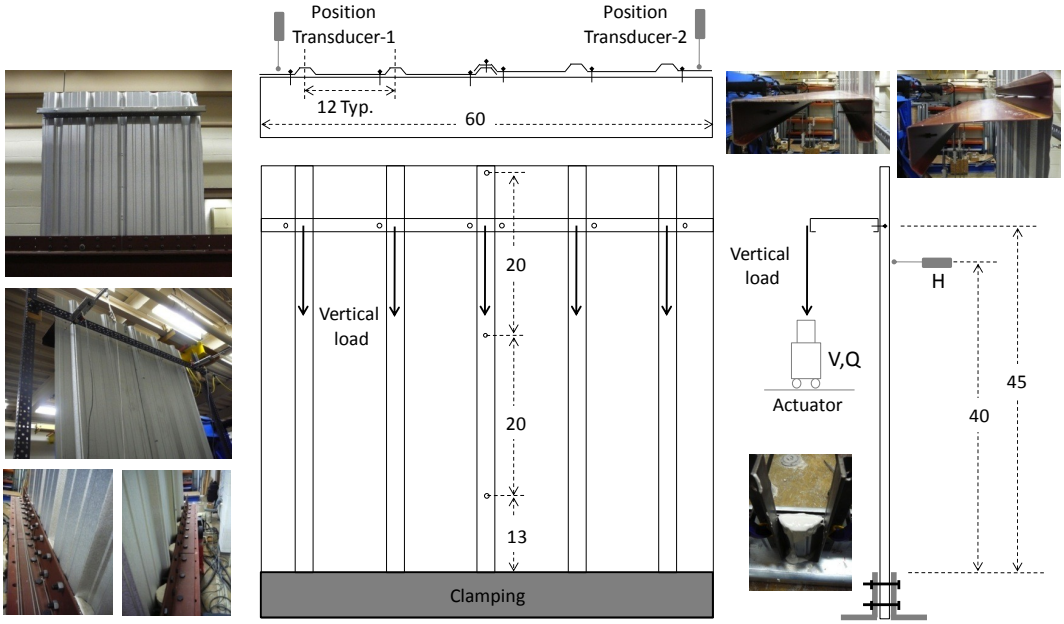

Figure 4: Test setup (all dimensions in *in.*)

2.2 Rotational restraint mechanical model

A mechanical model is developed to predict specimen stiffness and deflection observed in the experiments. The model configuration is shown in Figure 5. The total vertical deflection, V, is the sum of the vertical deflections caused by panel bending, web bending, flange bending and local panel pull-out (the spring in Figure 5). Deformations are assumed to be small.

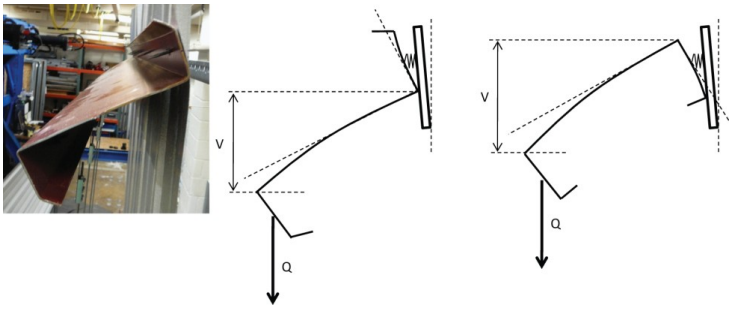

Figure 5: Rotational restraint mechanical model

Panel bending

As shown in Figure 6(a), the panel is a cantilever beam with a moment, *M*, applied at the free end via the member-panel connection.

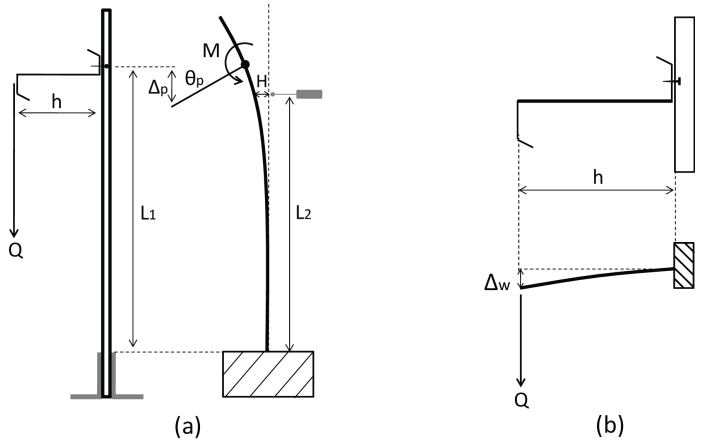

Figure 6: (a) Panel bending (b) Web bending

$$\Delta_p = h\theta_p \quad , \quad \theta_p = \frac{ML_1}{EI_p} \quad , \quad M = Qh \quad , \quad EI_p = \frac{ML_2^2}{2H}, \tag{1}$$

where EI_p is the panel stiffness; h is the member depth as shown in Table 1; H is the horizontal deflection measured by the position transducer; L_1=45 mm; L_2=40 mm. From Eqs. (1), the vertical deflection caused by panel bending is:

$$\Delta_p = \frac{9Hh}{160}. \tag{2}$$

Member web bending

The vertical deflection due to girt web bending can be calculated as:

$$\Delta_w = \frac{Qh^3}{3EI} \quad , \quad EI = 29500\frac{bt^3}{12}, \tag{3}$$

where EI is the member stiffness, E=29500 ksi and b is the girt length (60 in.).

Member flange bending

Notice that the member flanges are bent due to the loading Q depending on the member profile (Zee or Cee) as shown in Figure 7(a) and (c). Their models for the calculation are shown in Figure 7(b) and (d) respectively. It is assumed that the corner between the web and flange remains 90^o under loading. Thus, the flange is calculated as a cantilever beam.

In the Figure 7 (b),

$$\Delta_{f-z} = \theta_{f-z}h \quad , \quad \theta_{f-z} = \frac{\delta}{C} \quad , \quad \delta = \frac{FC^3}{3EI} \quad , \quad F = \frac{Qh}{C}, \tag{4}$$

where EI is the member stiffness as calculated in Eq. (3). The flange deflection, δ, is that created

by force F in the fastener. From Eq. (4), the vertical deflection from Zee member flange bending is calculated as:

$$\Delta_{f-z} = \frac{Qh^2C}{3EI}. \tag{5}$$

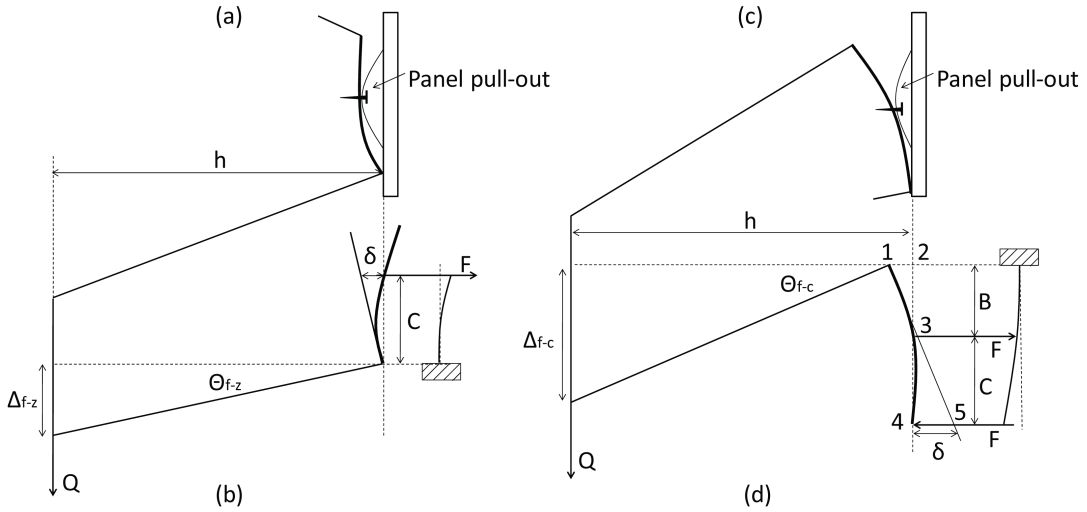

Figure 7: (a) Zee flange bending (b) Zee flange model (c) Cee flange bending (d) Cee flange model

In the Figure 7(d), ∠132=∠435, where the line-15 is perpendicular to the web, and point-3 is the intersection of the line-24 and line-15. The length of the line-34 is approximately equal to C (see Figure 3), and therefore:

$$\Delta_{f-c} = \theta_{f-c}h \quad , \quad \theta_{f-c} = \frac{\delta}{C} \quad , \quad \delta = \frac{F\left(\frac{B^2C}{2} + BC^2 + \frac{C^3}{3}\right)}{EI}, \tag{6}$$

where EI and F are calculated in Eq. (3) and (4) respectively. From Eqs. (6), the vertical deflection due to the Cee member flange bending is calculated as:

$$\Delta_{f-c} = \frac{Qh^2\left(\frac{B^2C}{2} + BC^2 + \frac{C^3}{3}\right)}{EIC^2}. \tag{7}$$

Panel pull-out spring behavior

The screws pull the panel out as shown in Figure 8(a). The panel pull-out is represented by a linear spring, and its stiffness k (for each screw) is obtained from a linear elastic finite element analysis as shown in Figure 8(b). The base of the panel was fully fixed in 6 directions (1, 2, 3, R1, R2 and R3) and the corner (of flange and web) bearing was also simulated by fixing the 1 direction.

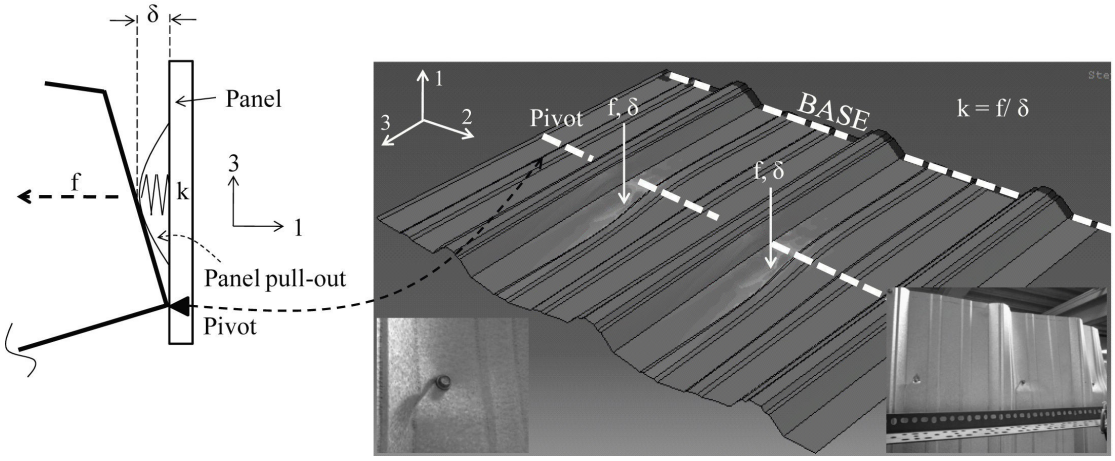

(a) (b)

Figure 8: Panel pull-out (a) calculation model (b) ABAQUS simulation

The panel pull-out stiffness k is influenced by C defined in Figure 3. For a particular C, k is taken as the slope of f versus δ as shown in Figure 9 (a). The function $k(C)$ is calculated using the trending line as shown in Figure 9(b).

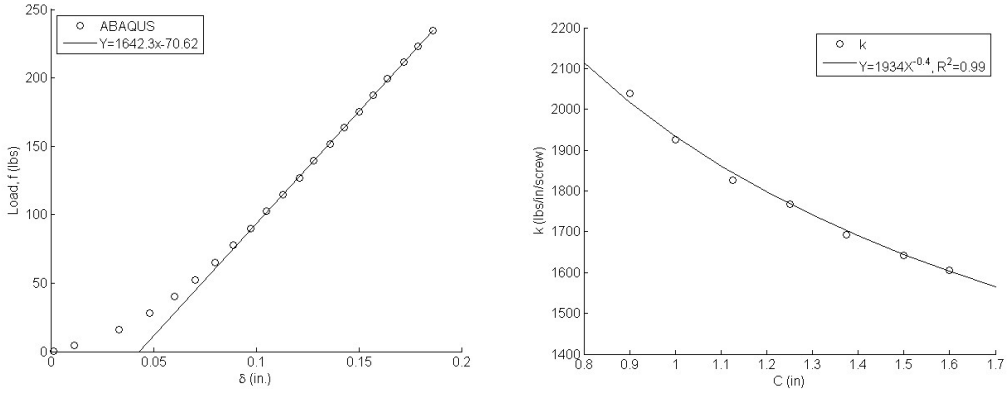

(a) (b)

Figure 9: Panel pull-out stiffness at each fastener (a) k at C=1.5 in. (b) function $k(C)$.

The vertical deflection due to the panel pull-out is then calculated as shown in Figure 8(a) where K is the stiffness of the total 6 screws (K=6k):

$$\Delta_s = \theta_s h \quad , \quad \theta_s = \frac{\delta}{C} \quad , \quad \delta = \frac{F}{K}, \tag{8}$$

and where F is calculated in Eq. (4). From Eqs. (8), the vertical deflection is calculated as:

$$\Delta_s = \frac{Qh^2}{KC^2}. \tag{9}$$

By combining Eq. (2), (3), (5), (7), and (9), the vertical displacement V is calculated for a Zee section as:

$$V_z = Q\left(\frac{h^2}{KC^2} + \frac{h^2 C}{3EI} + \frac{h^3}{3EI}\right) + \frac{9Hh}{160}, \tag{10}$$

and for a Cee section:

$$V_c = Q\left(\frac{h^2}{KC^2} + \frac{h^2\left(\frac{B^2C}{2} + BC^2 + \frac{C^3}{3}\right)}{EIC^2} + \frac{h^3}{3EI}\right) + \frac{9Hh}{160}. \tag{11}$$

2.3 Comparison of experimental results and mechanical model

The mechanical model is now compared to the rotational restraint test results. Since *H* in the second term in Eqs. (10) and (11) is directly measured by the position transducers (see Figure 4), the *9Hh/160* is subtracted from both Eq.s (10) and (11) and the experimental results for the comparison.

Excellent agreement between the mechanical model and experimental results is observed in Figure 10 except for a slight difference in specimen C6-1. The discrepancy may be due to the large deformation in C6-1 (remember t=0.069 in. for this specimen) which violates the assumption of the small deformation in the mechanical model.

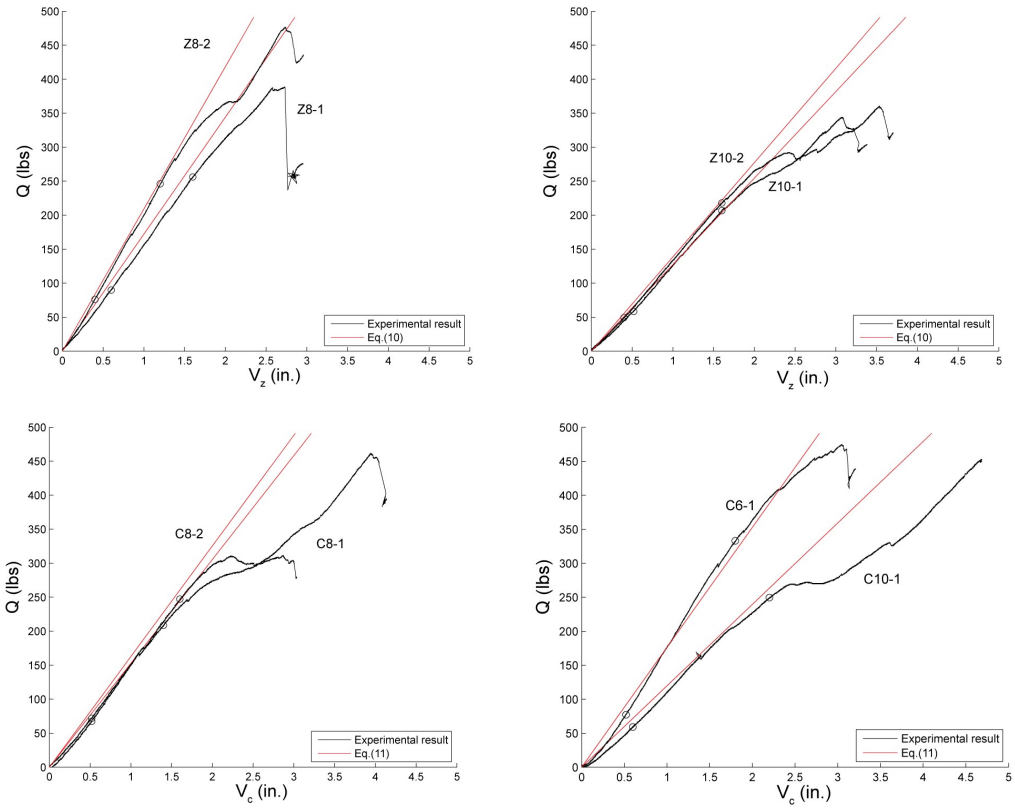

Figure 10: Comparison of mechanical model predictions and rotational restraint results

The slopes of the linear region (between 'o's in Figure 10) in the experimental results are compared to the prediction model (Table 2). Except for C6-1, the difference between the predicted stiffness and experimental results is less than 5%.

Table 2: Comparison of the predicted and experimental stiffness in Figure 10

Specimen name	Model slope (a) N/mm	Test slope (b) N/mm	a/b 100.0%
Z8-1	173.3	164.4	105.4
Z8-2	210.6	211.1	99.7
Z10-1	128.3	135.6	94.5
Z10-2	139.4	138.9	100.5
C8-1	153.9	153.3	100.2
C8-2	163.9	164.4	99.6
C10-1	120.6	117.8	102.5
C6-1	177.8	197.8	89.8

2.4 Girt-panel rotational stiffness

A calculation procedure for rotational stiffness can be derived from the mechanical model introduced in the previous section. The unit rotational stiffness, K_o (lbs.in/rad/in), is treated as the ratio of the unit moment M_u (lbs.in/in) applied at the corner of the flange and web to the rotation (rad) of the web as shown in Figure 11. The rotation is caused by flange bending and panel pull-out.

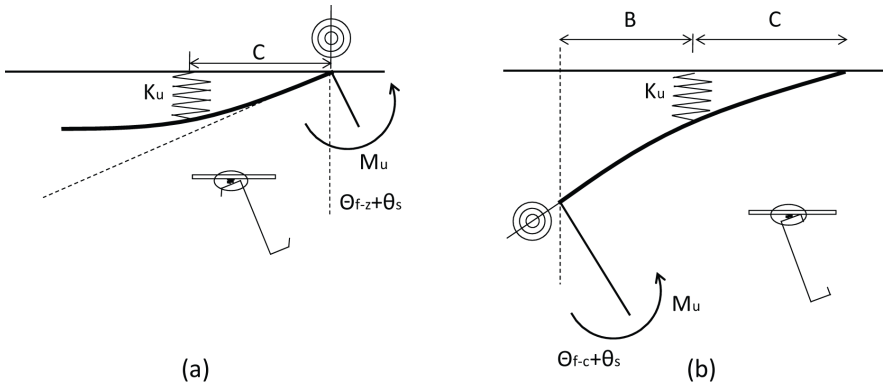

Figure 11: Model to calculate the unit rotational stiffness *Ko* (lbs-in/rad/in) in a (a) Zee (b) Cee.

The rotation $\theta_{f\text{-}z}+\theta_s$ and $\theta_{f\text{-}c}+\theta_s$ were calculated in Eq. (4), (6) and (8) where $Qh=M_u$ in Eq. (4). For a member with a Zee cross-section,

$$K_{o-z} = \frac{M_u}{\theta_{f-z} + \theta_s} = \frac{1}{\frac{1}{K_u C^2} + \frac{C}{3EI_u}} \tag{12}$$

For a Cee section,

$$K_{o-c} = \frac{M_u}{\theta_{f-c} + \theta_s} = \frac{1}{\frac{1}{K_u C^2} + \frac{\frac{B^2 C}{2} + BC^2 + \frac{C^3}{3}}{EI_u C^2}} \tag{13}$$

where K_u is the unit panel pull-out stiffness, and EI_u is the unit member flexural rigidity. The

rotational stiffness, K_o, shown in Table 3 is calculated based on the dimensions and details in Table 1. Generally, K_o of a Cee section is lower than a Zee section, which is a potential contributor to the lower girt capacities of Cees compared to Zees observed in experiments.

Table 3: K_o calculated based on Table 1

Specimen name	Z8-1	Z8-2	Z10-1	Z10-2
K_o (kips.in/rad/in)	0.19	0.25	0.24	0.27
Specimen name	C8-1	C8-2	C10-1	C6-1
K_o (kips.in/rad/in)	0.17	0.18	0.22	0.13

2.5 Summary and discussion

In this study, a mechanical model was derived to predict the rotational stiffness at a girt-panel connection. The prediction had an excellent agreement with the experimental results. In the future, a rotational spring stiffness representing panel-to-girt rotational restraint could be calculated and then input into the finite strip method to predict girt capacity with the AISI Direct Strength Method as discussed in Appendix A.

3. Panel-Insulation-Girt Rotational Restraint

3.1 Experiments

The same rotational restraint test setup discussed in Section 2.1 was also employed to evaluate rotational stiffness of wall systems including fiberglass blanket and rigid board insulation. The girts and wall panel dimensions are the same as those described in Figure 3, Figure 4, and Table 1. Of particular interest in this study was the influence of rigid board insulation thickness on rotational restraint. Also, two different types of rigid board insulation were considered, Thermax and XPS. The rotational restraint test matrix is provided in Table 4.

Table 4: Testing matrix and specimen details

Specime name	Member Profile	Member depth, h (in.)	Insulation type	Insulation thickness (in.)	Average B (in.)	Average C (in.)	Thickness bare, t (in.)
Z8-R-1	Z	8	R13	4	---	1.17	0.103
Z8-R-2	Z	8	R13	4	---	1.23	0.103
Z10-R-1	Z	10	R13	4	---	1.50	0.106
Z10-R-2	Z	10	R13	4	---	1.65	0.105
C6-TH2-1	C	6	Thermax	2	0.82	1.18	0.071
C8-TH2-1	C	8	Thermax	2	1.11	1.40	0.103
C8-TH2-2	C	8	Thermax	2	1.18	1.32	0.103
C10-TH2-1	C	10	Thermax	2	1.55	1.47	0.104
C10-TH2-2	C	10	Thermax	2	1.43	1.59	0.104
Z8-TH1-1	Z	8	Thermax	1	---	1.36	0.103
Z8-TH1-2	Z	8	Thermax	1	---	1.40	0.102
Z8-TH2-1	Z	8	Thermax	2	---	1.28	0.102
Z8-TH2-2	Z	8	Thermax	2	---	1.41	0.103
Z8-TH4-1	Z	8	Thermax	4	---	1.54	0.102
Z8-TH4-2	Z	8	Thermax	4	---	1.35	0.103
Z8-XPS1-1	Z	8	XPS	1	---	1.58	0.103
Z8-XPS2-1	Z	8	XPS	2	---	1.39	0.103
Z8-XPS4-1	Z	8	XPS	4	---	1.56	0.102

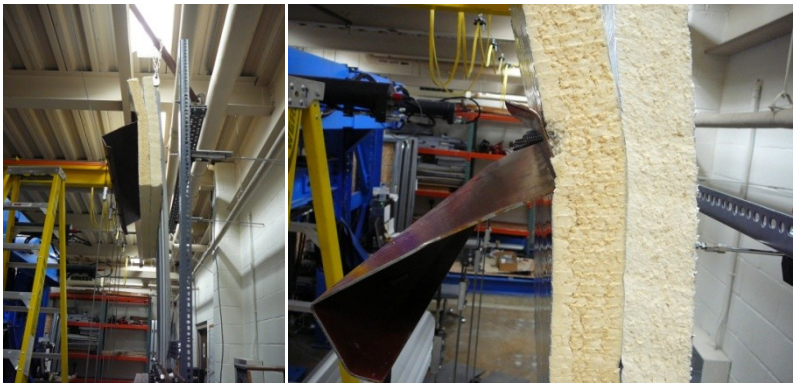

Figure 12: Rotational restraint test with rigid board insulation

3.2 Rigid board material properties

The compressive stress-strain behavior of both Thermax and XPS insulation were obtained experimentally using 2 in. thick specimens and a two post uniaxial testing machine. The results in Figure 13 demonstrate that Thermax and XPS have quite different compressive behavior. Thermax exhibited a yield plateau at approximately 23 psi, while XPS was stiffer, deforming with gradually yielding behavior and no distinct yield point. Both Thermax and XPS have tri-linear stress-strain curves. The rigid board deforms linear elastically until the cell walls buckle and the material loses stiffness. Stiffness increases again after the foam cells have completely collapsed. It is hypothesized that the rigid board stress-strain behavior should affect rotational restraint provided to the girt, especially at the girt rotational pivot point where contact pressure is high, see Figure 12. This hypothesis will be addressed in the following sections.

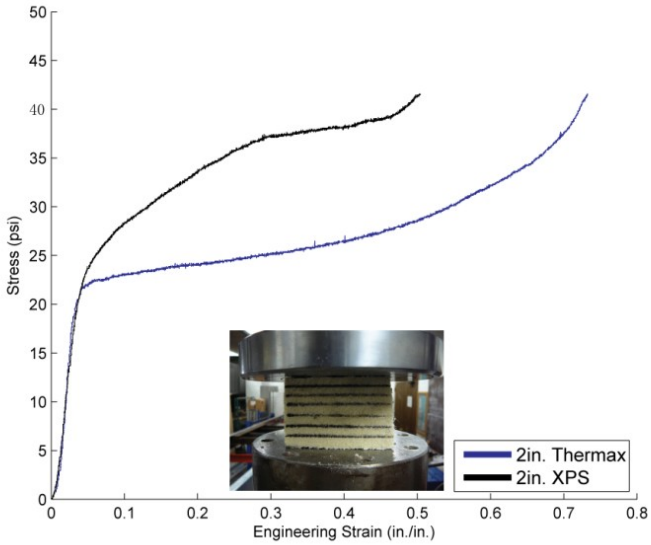

Figure 13: Compression test of 2 in. rigid board

3.3 Rotational restraint test results

For the study of girt-panel rotational restraint tests in Section 2.3, it was demonstrated that the total vertical deflection *V* (see Figure 4) is caused by web bending, flange bending, panel pull out and panel bending. The same effects act for the tests considered in this section, however insulation indentation also plays an important role as illustrated in Figure 14. Unfortunately, it is difficult to include the foam indentation in the calculations described in Section 2.2 because of the complex nonlinear interaction between the insulation and the girt. Therefore, the objective of section is simply to compare the effect of rigid board type (Thermax and XPS), insulation thickness, and girts cross-section on rotational restraint. Note that for all results in the following sections, the average fastener location in the flange, *C*, defined in Figure 3, is provided along with the load-deformation response. This is because rotational restraint increases as the moment arm between the pivot point and the screw fastener increases, i.e., rotational restraint increases as *C* increases.

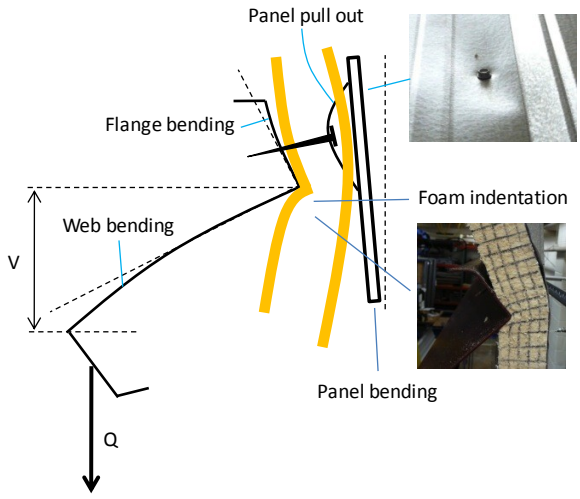

Figure 14: Components of vertical displacement V

3.4 Effect of rigid board thickness

The results of 8 in. deep Zee girts with different thickness of rigid board insulation are plotted in Figure 15. Tri-linear behavior is observed in the load-deformation response (note initially stiff response, then softer response, then stiffer response), which is consistent with the compressive stress-strain behavior in Figure 13. If rotational restraint is represented as the slope of the load-deformation response, then it is clear from Figure 15 that for both XPS and Thermax, the stiffness increases as a function of rigid board thickness, compare Z8TH1-1 with 1 in. thick Thermax insulation to Z8-TH4-1 with 4 in. of Thermax insulation in Figure 15a. The rigid board improves rotational restraint by acting as a washer to reinforce the panel at the fastener location, reducing local panel deformation and preventing panel pullover in most cases where insulation was present. Note that the tests with fiberglass insulation (Z8-R-1 and Z8-R-2 in Figure 15b) act more like the bare panel case because the insulation is compressible and does not provide any appreciable reinforcement to the metal panel.

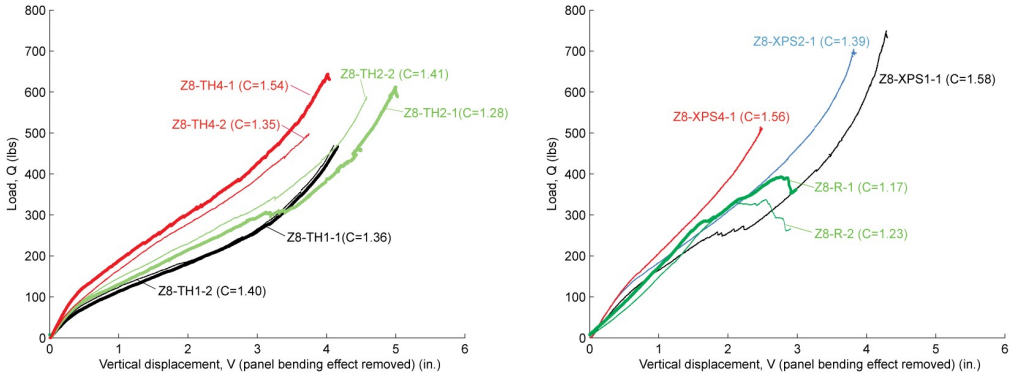

(a) (b)

Figure 15: Effect of rigid board thickness (a) Thermax (b) XPS on the rotational restraint

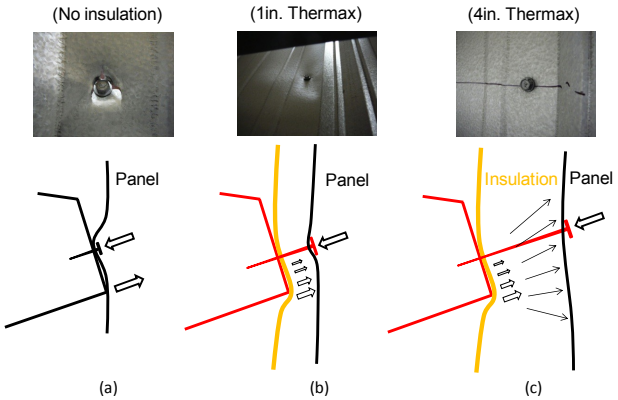

Figure 16: Washer behavior provided by rigid board insulation to the metal panel

3.5 Effect of cross-section dimensions

The results for the 8 in. deep Cee and Zee girts with 2 in. of Thermax rigid board insulation are compared in Figure 17. There is a minimal difference in the first two linear regions of the Cee and Zee loading curve, however the Cee shows less insulation hardening in the third linear region (compare Z8-TH2-2 to C8-TH2-1). It his hypothesized that since the bearing (pivot) points on a Cee and Zee are different (see Figure 7), that the pressure acting at the pivot point may vary also. According to this hypothesis, the Zee is bearing with a higher pressure than the Cee.

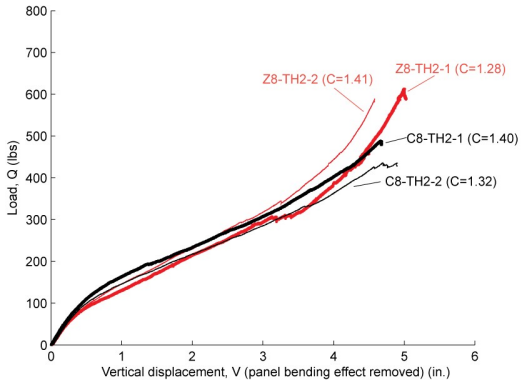

Figure 17: Effect of cross-section type on rotational restraint

3.6 Effect of web depth

The effect of web depth on rotational restraint is summarized in Figure 18. It is not surprising that the deeper girts (10 in.) have less stiffness than the shallow ones (8 in.), compare C8-TH2-1 to C10-TH2-1. The results emphasizes that the girt is susceptible to cross-section deformation when the web is deeper, causing the free flange, i.e., the flange under compression in the wall system for a suction loading, to have larger laterally deformation in deeper web girts.

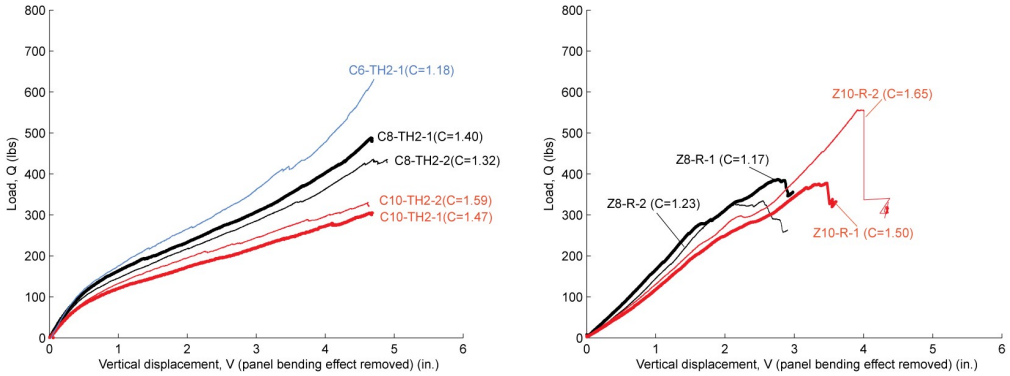

Figure 18: Effect of web depth on rotational restraint

3.7 Effect of insulation type (Thermax vs. XPS)

Figure 15(a) and (b) are merged in Figure 17 to compare the rotational restraint provided by Thermax and XPS. The XPS insulation provides higher rotational restraint than Thermax because of the stiffer compressive stress-strain response (see Figure 13). It is concluded that rigid board compressive material properties affect rotational restraint, and this effect should be considered in modifications to the current girt strength prediction procedures.

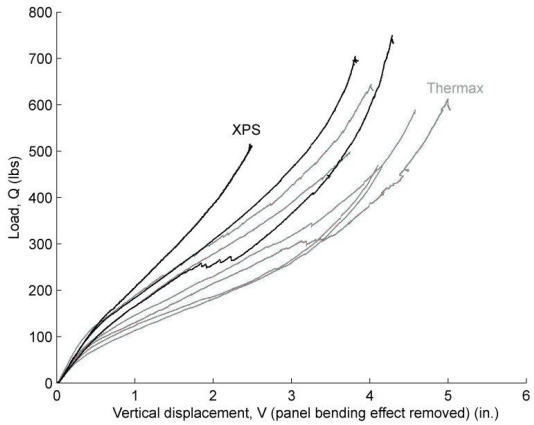

Figure 19: Effect of Thermax and XPS on rotational restraint

3.8 Comparison between rigid board and bare panel rotational restraint

Results of girt-panel (Section 2) and panel-rigid-board (Section 3) are plotted in Figure 20. The high variation between tests results from different insulation types, insulation thicknesses, web depths, cross-section types, and the fastener location *C*. However, meaningful conclusions can

still be drawn. Remember that rigid board insulation has three linear regions in its loading curve - elastic, plateau, and hardening. Before the rigid board insulation yields, the insulation provides a higher rotational restraint to the girts than the bare panel case. After yielding (plateau), the rigid board insulation provides less rotational restraint than the bare panel. After hardening initiates, the rigid board provided a higher rotational restraint to the Zee girts than the bare panel. The implications of these trends will be explored in the next section where wall systems with varying rigid board insulation thicknesses are tested to failure.

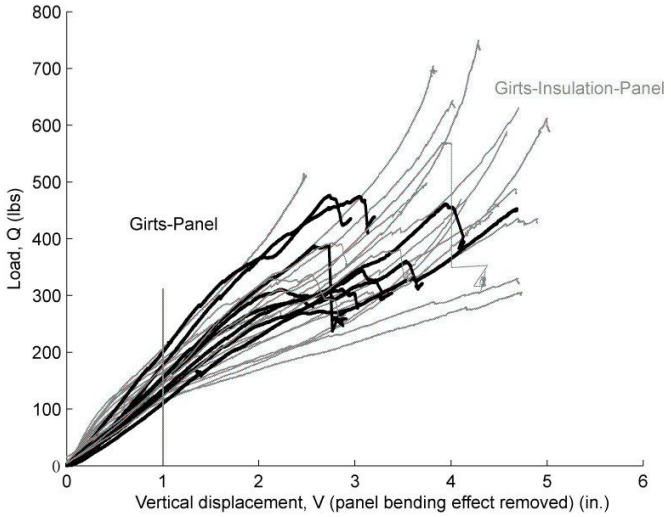

Figure 20: Comparison between bare panel and rigid board

4. Vacuum Box Tests of Girt Wall Assemblies

4.1 Test matrix

In this study, 50 vacuum box tests were conducted to investigate the influence of rigid board insulation on simple span girt flexural capacity. The experimental variables considered were girt cross-section (Z8, Z10, C8 and C10), wall panel type, and insulation type and thickness – fiberglass blankets and Thermax rigid board insulation (1 in. 2 in., and 4 in.). The test matrix is provided in Table 5.

4.2 Test setup

Each test was performed with two parallel girts through-fastened to metal panels at a fastener spacing of 12 in. One end of the each girt was supported on a roller, and the other on a pin, to ensure that the midspan moment ($wL^2/8$) could be accurately calculated. The centerline bearing to centerline bearing span was 24.5 ft, and the girt spacing was 7 ft out to out from web to web. The transverse panel span was purposely set at 13 ft-7 in. to produce panel deflections consistent with a continuous span. The panels were tested in an unconventional manner, i.e., upside down, so that girt deformation could be observed as air was pulled out from the bottom of the pressure box. The detailed construction procedure and figures describing the test boundary conditions are provided in Appendix B.

Table 5: Testing Matrix

#	Test name	Girt	Web in.	Panel	Insulation	Thickness in.
1	Z8D-1	Zee	8	D	None	0
2	Z8D-2				None	0
3	Z8D-3				None	0
4	Z8DR4-1				R13	4
5	Z8DR4-2				R13	4
6	Z8DTH1-1				Thermax	1
7	Z8DTH1-2				Thermax	1
8	Z8DTH2-1				Thermax	2
9	Z8DTH2-2				Thermax	2
10	Z8DTH4-1				Thermax	4
11	Z8DTH4-2				Thermax	4
12	Z8B-1			B	None	0
13	Z8B-2W				None	0
14	Z8BTH1-1				Thermax	1
15	Z8BTH1-2				Thermax	1
16	Z8BTH2-1				Thermax	2
17	Z8BTH2-2				Thermax	2
18	Z8BTH4-1				Thermax	4
19	Z10D-1		10	D	None	0
20	Z10D-2				None	0
21	Z10DTH1-1				Thermax	1
22	Z10DTH1-2				Thermax	1
23	Z10DTH2-1				Thermax	2
24	Z10DTH2-2				Thermax	2
25	Z10DTH4-1				Thermax	4
26	Z10DTH4-2				Thermax	4
27	Z10B-1			B	None	0
28	Z10B-2				None	0
29	Z10BTH1-1				Thermax	1
30	Z10BTH1-2				Thermax	1
31	Z10BTH2-1				Thermax	2
32	Z10BTH2-2				Thermax	2
33	Z10BTH4-1				Thermax	4
34	Z10BTH4-2				Thermax	4
35	C8D-1	Cee	8	D	None	0
36	C8D-2				None	0
37	C8DTH1-1				Thermax	1
38	C8DTH1-2				Thermax	1
39	C8DTH2-1				Thermax	2
40	C8DTH2-2				Thermax	2
41	C8DTH4-1				Thermax	4
42	C8DTH4-2				Thermax	4
43	C10D-1		10		None	0
44	C10D-2				None	0
45	C10DTH1-1				Thermax	1
46	C10DTH1-2				Thermax	1
47	C10DTH2-1				Thermax	2
48	C10DTH2-2				Thermax	2
49	C10DTH4-1				Thermax	4
50	C10DTH4-2				Thermax	4

4.3 Instrumentation

A set of two pressure transducers (Figure 21a, accuracy of +/-0.5 psf) were used to measure pressure inside the vacuum box. The transducers were calibrated with a water tube manometer. Wire potentiometers (WP) were used to measure the translation of the deflected flange as shown in Figure 21(b). They were mounted on an instrument bar as shown in Figure 22, allowing the measurement of vertical and horizontal displacements of points A and B (intersection of web and top flange) from a fixed datum. Two cameras recorded the video of each girt during a test (Figure 21c).

(a) (b) (c)

Figure 21: (a) Pressure transducer (b) wire potentiometers (WP) (c) video camera

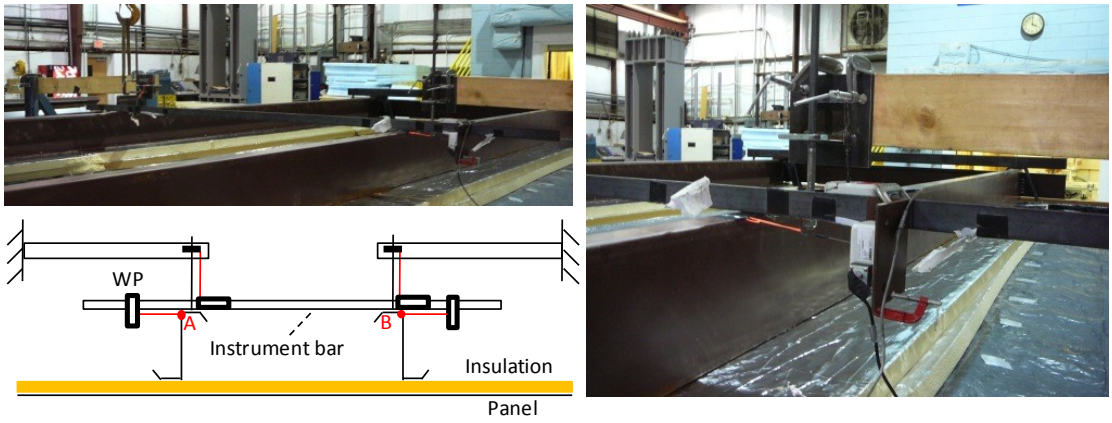

Figure 22: Instrumentation

4.4 Test procedure

Before recording data, the vacuum pump (Figure 23a) was turned on with all vents open for 1 minute to zero the pressure. Immediately after starting to record the data and video, two supplemental vacuums (Figure 23b) were turned on, and then the vents were closed manually in the order shown in Figure 23(c). The loading rate could not be finely controlled, however the loading histories plotted in Figure 24 demonstrate that the loading rate was slow (approximately 0.1 psf/sec) and constant.

(a) (b) (c)

Figure 23: (a) Vacuum pump, (b) Shop Vacs, (c) air vents

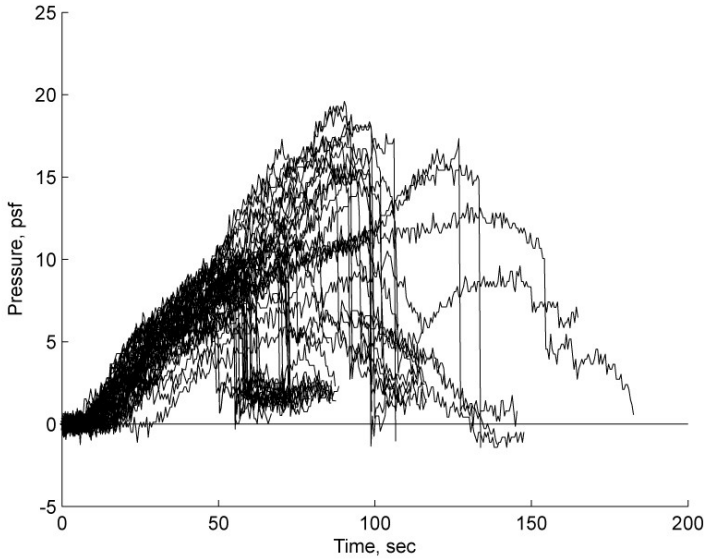

Figure 24: Loading history for all tests

Once a specimen failed, the vacuums and motor were turned off and the data and video were saved. The maximum pressure, *P*, was visually determined at the peak of the loading curve as shown in Figure 25. The pressure in Figure 25 is the average of two pressure transducers positioned inside the vacuum chamber.

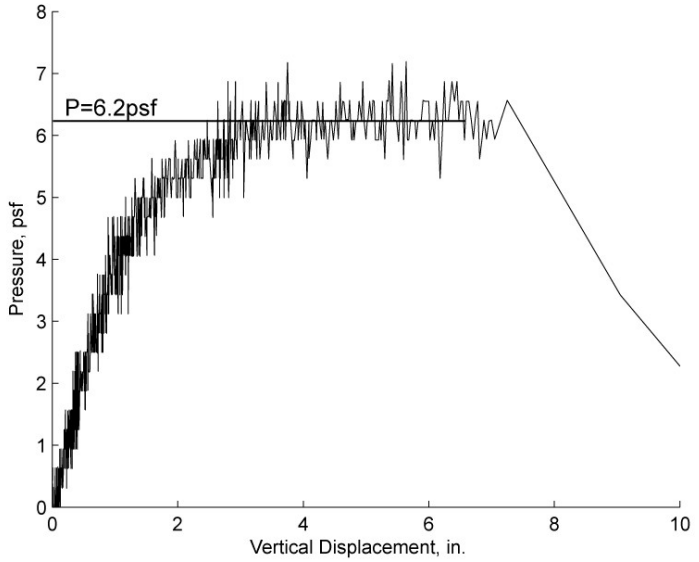

Figure 25: Loading versus vertical displacement of failed girt

The failure moment, M_t, was calculated as

$$\mathrm{D\,(lbs/in)} = \frac{\mathrm{P}}{144} \times \frac{L_p \times 12}{2} + \frac{d_p}{w \times 12 \times 12} + \frac{d_g}{L_g \times 12} \tag{14}$$

$$\mathrm{M_t\,(k\text{-}in)} = \frac{\mathrm{D} \times (\mathrm{L_g} \times 12)^{12}}{8} / 1000 \tag{15}$$

where the panel length, L_p=13.58 ft; the girt span, L_g=24.5 ft; the weight of a single metal panel d_p=35 lbs; the girt weight, d_g=118 lbs (Z8), 80 lbs (Z10), 114 lbs (C8), 78 lbs(C10); and the metal panel width, w=3 ft.

4.5 Material properties

The steel yield stress for each failed girt (only one of the two girts typically failed in a test) was determined with tensile coupon tests taken from the two flanges and web of an untested girt segment. The surface paint was removed with acetone and steel wool before measuring the base metal thickness. The average yield stress of three coupon specimens for each failed girt is summarized in Table 6. The yield stress of the two metal building panels considered, denoted **D** and **B,** were measured with one tensile coupon test each, resulting in 50 ksi and 80 ksi respectively.

Table 6: Tensile yielding stresses

Test name	Yield stress ksi
Z8D-2	60.97
Z8D-3	60.18
Z8DTH1-1	62.05
Z8DTH1-2	60.61
Z8DTH2-1	61.38
Z8DTH2-2	61.71
Z8DTH4-1	61.89
Z8DTH4-2	61.00
Z8D4R13-1	62.05
Z8D4R13-2	60.60
Z8B-1	62.76
Z8B-2W	60.58
Z8BTH1-1	61.03
Z8BTH1-2	60.98
Z8BTH2-1	61.53
Z8BTH2-2	61.50
Z8BTH4-1	61.01

Test name	Yield stress ksi
Z10D-1	58.49
Z10D-2	58.09
Z10DTH1-1	58.53
Z10DTH1-2	59.30
Z10DTH2-1	58.80
Z10DTH2-2	58.35
Z10DTH4-1	57.62
Z10DTH4-2	59.35
Z10B-1	58.21
Z10B-2	57.88
Z10BTH1-1	58.35
Z10BTH1-2	57.69
Z10BTH2-1	57.73
Z10BTH2-2	58.35
Z10BTH4-1	56.29
Z10BTH4-2	59.38

Test name	Yield stress ksi
C8D-1	75.73
C8D-2	75.34
C8DTH1-1	76.16
C8DTH1-2	76.31
C8DTH2-1	74.52
C8DTH2-2	76.95
C8DTH4-1	78.44
C8DTH4-2	79.38
C10D-1	61.30
C10D-2	60.06
C10DTH1-1	59.57
C10DTH1-2	59.42
C10DTH2-1	59.93
C10DTH2-2	59.85
C10DTH4-1	60.42
C10DTH4-2	59.94

4.6 Specimen dimensions

4.6.1 Girts

The girt types considered were Z8, Z10, C8 and C10, where the number denotes the out-to-out web height. Cross-section dimensions and sweep imperfections were measured at midspan before testing (Table 7). The effective section modulus, S_e, was calculated with the commercial software CFS.

Table 7: Cross section and imperfection of specimens

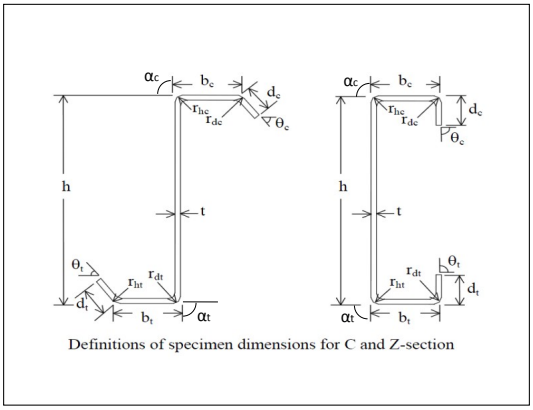

Definitions of specimen dimensions for C and Z-section

Specimen	Cross-section												Girt
	Compression				Tension				h	r	t	S_e	Imperfection at mid span
	b	d	α	θ	b	d	α	θ					
	in.	in.	deg	deg	in.	in.	deg	deg	in.	in.	in.	$in.^3$	in.
Z8D-2	2.69	1.04	92	47	2.85	1.08	92	53	8	0.26	0.102	3.57	-
Z8D-3	2.68	0.99	91	47	2.58	1.01	90	53	8	0.32	0.100	3.50	-
Z8DTH1-1	2.78	1.00	92	46	2.79	1.10	91	52	8	0.28	0.100	3.50	-
Z8DTH1-2	2.60	1.04	90	47	2.73	1.04	89	53	8	0.25	0.100	3.59	-
Z8DTH2-1	2.89	0.95	91	48	2.73	1.03	90	53	8	0.30	0.101	3.39	-
Z8DTH2-2	2.71	1.03	91	47	2.63	0.84	91	52	8	0.41	0.101	3.36	-
Z8DTH4-1	2.75	0.89	92	47	2.76	1.05	90	53	8	0.30	0.101	3.32	-
Z8DTH4-2	2.74	0.99	90	46	2.79	1.12	90	54	8	0.27	0.102	3.49	-
Z8D4R13-1	2.68	0.99	90	48	2.68	1.09	90	53	8	0.22	0.100	3.51	-
Z8D4R13-2	2.67	1.01	90	47	2.67	1.04	90	52	8	0.25	0.099	3.55	-
Z8B-1	2.70	0.96	90	47	2.76	1.10	90	52	8	0.29	0.101	3.47	-
Z8B-2W	2.68	1.02	91	46	2.76	1.03	91	53	8	0.26	0.101	3.56	0.01
Z8BTH1-1	2.76	1.03	90	46	2.77	1.09	88	53	8	0.24	0.100	3.56	-
Z8BTH1-2	2.71	1.05	91	46	2.68	1.05	91	53	8	0.26	0.100	3.59	-
Z8BTH2-1	2.84	0.99	89	48	2.81	1.10	89	53	8	0.30	0.101	3.49	-
Z8BTH2-2	2.68	0.99	90	47	2.70	1.05	90	53	8	0.31	0.101	3.54	-
Z8BTH4-1	2.68	1.02	90	47	2.71	0.99	90	52	8	0.27	0.101	3.51	-0.21
Z10D-1	2.83	0.78	90	55	2.89	0.80	91	46	10	0.28	0.060	2.19	0.00
Z10D-2	2.83	0.82	90	55	2.86	0.84	90	48	10	0.25	0.060	2.21	0.07
Z10DTH1-1	2.69	0.79	92	54	2.91	0.82	91	47	10	0.25	0.059	2.16	-
Z10DTH1-2	2.66	0.74	91	55	2.86	0.80	90	47	10	0.22	0.059	2.12	-
Z10DTH2-1	2.65	0.83	90	54	2.83	0.81	91	47	10	0.26	0.061	2.18	-0.15
Z10DTH2-2	2.83	0.79	91	56	2.87	0.81	91	47	10	0.25	0.061	2.18	0.11
Z10DTH4-1	2.83	0.86	91	55	2.82	0.78	90	48	10	0.27	0.060	2.30	0.08
Z10DTH4-2	2.84	0.87	90	54	2.87	0.79	90	46	10	0.24	0.060	2.23	0.33
Z10B-1	2.82	0.83	91	55	2.87	0.87	90	47	10	0.23	0.059	2.20	-0.01
Z10B-2	2.78	0.88	91	54	2.88	0.80	91	47	10	0.24	0.059	2.24	-0.12
Z10BTH1-1	2.94	0.87	91	55	2.76	0.85	91	47	10	0.24	0.059	2.27	0.21
Z10BTH1-2	2.73	0.80	90	55	2.86	0.79	89	47	10	0.25	0.060	2.23	0.06
Z10BTH2-1	2.73	0.75	90	55	2.80	0.81	90	48	10	0.23	0.060	2.12	0.00
Z10BTH2-2	2.68	0.76	90	55	2.75	0.78	90	48	10	0.22	0.060	2.13	0.15
Z10BTH4-1	2.68	0.71	90	53	2.87	0.79	88	45	10	0.20	0.060	2.08	0.25
Z10BTH4-2	2.68	0.89	90	54	2.87	0.80	88	47	10	0.27	0.060	2.27	0.12
C8D-1	2.57	0.84	92	90	2.56	0.85	92	90	8	0.20	0.101	3.11	-0.51
C8D-2	2.59	0.84	88	90	2.54	0.84	88	90	8	0.23	0.101	3.11	-0.33
C8DTH1-1	2.51	0.83	93	90	2.54	0.83	93	90	8	0.19	0.101	3.11	-0.40
C8DTH1-2	2.63	0.80	92	90	2.54	0.82	92	90	8	0.18	0.101	3.04	-0.50
C8DTH2-1	2.42	0.83	91	90	2.47	0.79	91	90	8	0.16	0.101	3.11	-0.49
C8DTH2-2	2.45	0.79	88	90	2.68	0.85	88	90	8	0.23	0.101	3.07	-0.33
C8DTH4-1	2.55	0.83	87	90	2.59	0.83	87	90	8	0.25	0.101	3.08	-0.41
C8DTH4-2	2.54	0.84	88	91	2.56	0.83	88	91	8	0.18	0.101	3.07	-0.31
C10D-1	2.54	0.82	90	89	2.58	0.77	90	89	10	0.22	0.059	2.06	0.01
C10D-2	2.51	0.82	89	91	2.56	0.76	89	91	10	0.22	0.059	2.07	-0.12
C10DTH1-1	2.49	0.83	89	90	2.49	0.82	89	90	10	0.17	0.059	2.09	-0.20
C10DTH1-2	2.48	0.82	89	89	2.54	0.80	89	89	10	0.17	0.059	2.08	-0.13
C10DTH2-1	2.48	0.79	90	90	2.68	0.84	90	90	10	0.19	0.059	2.04	-0.01
C10DTH2-2	2.49	0.83	90	90	2.71	0.75	90	90	10	0.22	0.059	2.08	0.01
C10DTH4-1	2.52	0.78	90	89	2.57	0.75	90	89	10	0.17	0.059	2.03	0.08
C10DTH4-2	2.47	0.82	90	91	2.56	0.71	90	91	10	0.19	0.059	2.07	0.10

4.6.2 Panel

The two panel cross-sections considered are shown in Figure 26. Panel **D** is 1-1/8" deep, while Panel **B** is 1-1/4" deep.

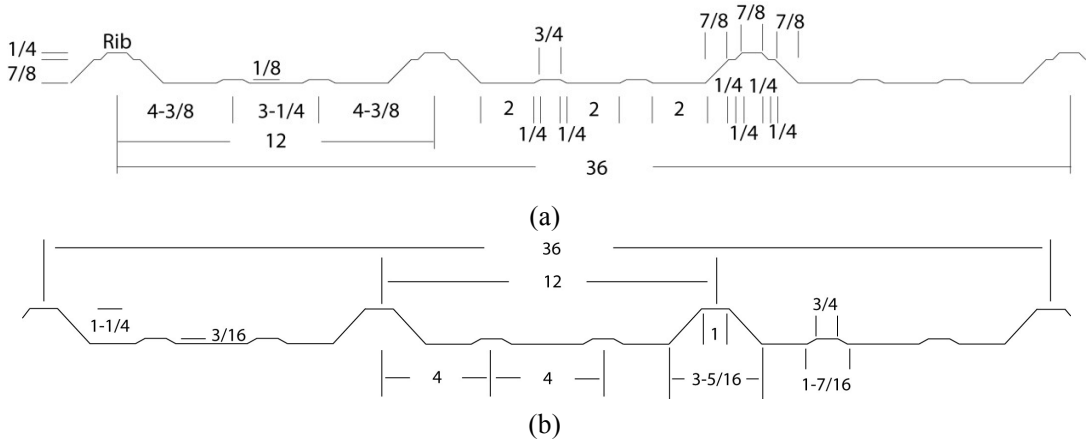

Figure 26: (a) Cross-section of panel D; (b) Cross-section of panel B (all dimensions in in.)

4.6.3 Screw fasteners

Two sizes of screws without washers were used: 5 in. #1/4-14 self drilling screw for the test specimens with 4 in. of rigid board insulation; #12 screws for all other test specimens. The diameter of #1/4-14 and #12 screws are 0.211 in. and 0.182 in. respectively. In test Z8B-2W, #12 screws with a washer were used as shown in Figure 27. All screws were installed directly next to the rib every 12 in. on center as shown in Figure 28.

Figure 27: Screw with washer

Figure 28: Fastener location

It was demonstrated in Section 2 that rotational restraint provided to the girt depends on the screw location *C*, which is the distance between the girt bearing pivot point and the center of screw hole (see Figure 3). Since the girt capacity was expected to sensitive to *C*, it was measured after each test. Specifically, the distance between the pivot point and the hole edge, *e*, was

measured with digital caliper (Figure 29) on failed girts over the middle half of the span. Screw location, *C*, reported in Table 8, is the average *e* plus half the screw diameter, *d*/2, as shown in Figure 31.

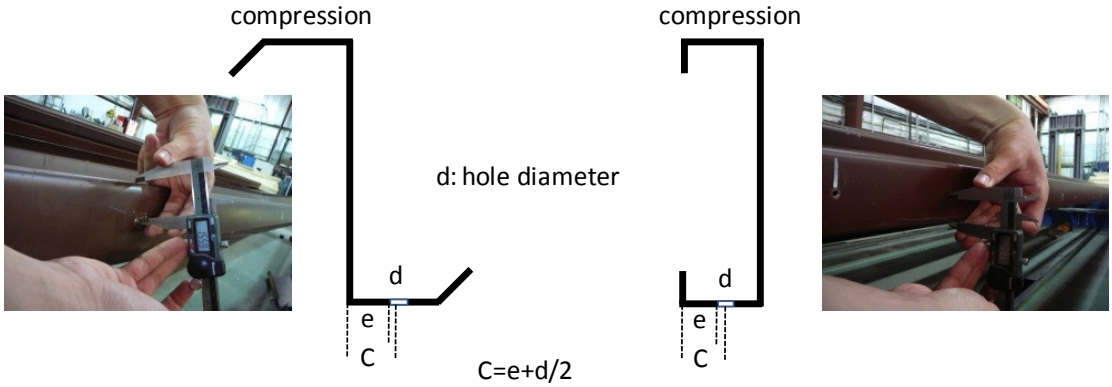

Figure 29: Screw location C determination

Table 8: Average screw location C at failed girts in each test

Specimen	C in.	Specimen	C in.	Specimen	C in.	Specimen	C in.	Specimen	C in.
Z8D-1	NA	Z8DTH4-2	2.10	Z10DTH1-1	1.53	Z10BTH2-1	1.63	C8DTH4-1	1.01
Z8D-2	1.54	Z8B-1	1.62	Z10DTH1-2	1.41	Z10BTH2-2	1.53	C8DTH4-2	0.47
Z8D-3	1.47	Z8B-2W	1.42	Z10DTH2-1	1.09	Z10BTH4-1	1.45	C10D-1	0.79
Z8DR4-1	1.58	Z8BTH1-1	1.65	Z10DTH2-2	1.19	Z10BTH4-2	1.59	C10D-2	1.10
Z8DR4-2	0.82	Z8BTH1-2	1.24	Z10DTH4-1	1.74	C8D-1	1.33	C10DTH1-1	0.85
Z8DTH1-1	1.46	Z8BTH2-1	1.86	Z10DTH4-2	1.23	C8D-2	1.04	C10DTH1-2	1.30
Z8DTH1-2	1.78	Z8BTH2-2	1.59	Z10B-1	0.98	C8DTH1-1	0.79	C10DTH2-1	0.85
Z8DTH2-1	1.47	Z8BTH4-1	1.35	Z10B-2	1.66	C8DTH1-2	1.03	C10DTH2-2	0.49
Z8DTH2-2	1.41	Z10D-1	1.36	Z10BTH1-1	1.06	C8DTH2-1	0.83	C10DTH4-1	0.85
Z8DTH4-1	1.11	Z10D-2	1.20	Z10BTH1-2	1.53	C8DTH2-2	0.96	C10DTH4-2	1.18

4.7 General observations

The first test, Z8D-1, failed due to panel bending (Figure 30a). Since the primary objective of this project was to quantify girt capacity, for all other tests the panels were stiffened at the middle as shown in Figure 30(b). Note that the girt flange was through fastened to a single panel, and therefore it is assumed that the reinforcement did not interfere with the connection zone. The influence of the experimental variables on girt capacity are summarized in the following sections.

(a) (b)

Figure 30: (a) Panel failure at midspan (b) stiffened panel at midspan

4.7.1 Screw location C

Girt capacity is very sensitive to screw location *C*. For example, in Figure 31, when *C* decreased from 2.10 in. to 1.11 in. for the same specimen type (Z8, D panel, 4 in. of Thermax) the maximum pressure at failure decreased by 30%. More girt rotation was observed in the test with C=1.11 in.

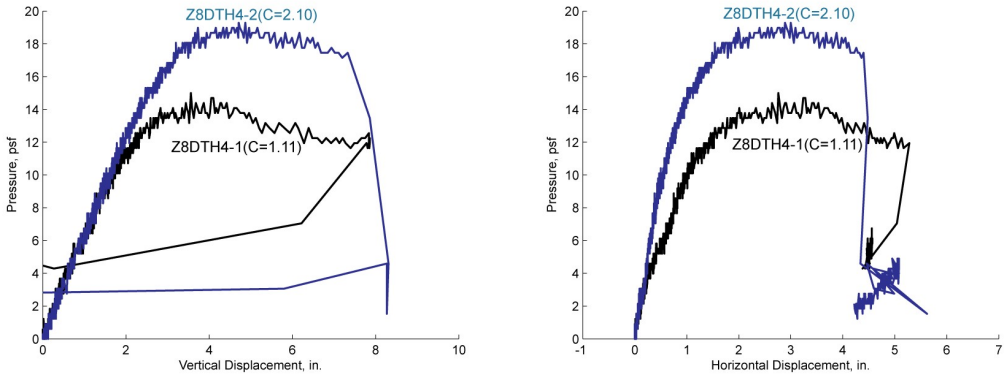

Figure 31: Effect of screw location C on girt load-deformation response

4.7.2 Cee vs. Zee

The horizontal displacement at mid span of the compression flange in all 10 in. deep Zee and Cee girts is plotted in figure 32. It is concluded that Cee girts rotated more (horizontal displacement/member depth=rotation) than Zee girts. It is hypothesized that the Cee sections propensity for rotation is related to the larger shear center offset (*m* in Figure 32) than in Zee sections, resulting in torsional moment that twists the cross-section.

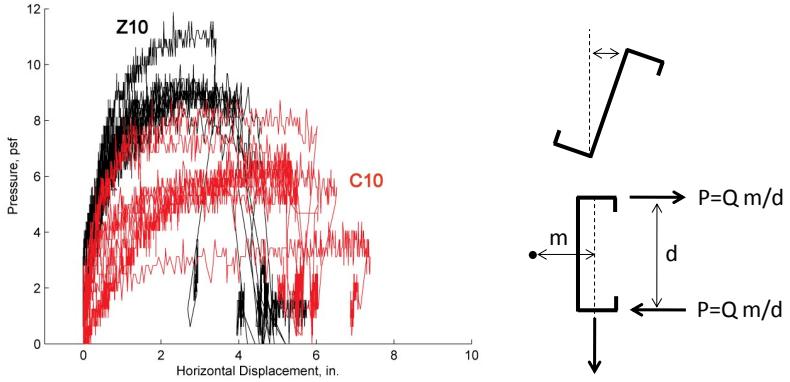

Figure 32: Horizontal displacement of 10 in. deep member

4.8 Failure modes

4.8.1 Zee girts (8 in. deep, 0.100 in. thick)

The common failure mode for Zee section girt specimens with locally stocky, rigid cross-sections was panel pull-over (Mode 2 in Table 9). In the case of bare panel (both D and B panel) and fiberglass blanket insulation, the panel pulled over the screw heads suddenly due to the girt rotation. As shown in Figure 33, there is little permanent deformation in the girts.

Figure 33: Screw pull over failure in bare panel tests

When rigid board insulation was added, the failure mode changed to a combination of panel pull-over, bent and/or broken screws, and girt yielding as shown in Figure 34. Screw bending was initiated by the presence of rigid board insulation as illustrated in Figure 35 because of the distance (=board thickness) between girts and panel, which allowed the girt to rotate and create a concentrated moment that could be resisted by the thick 0.1 in. base metal thickness.

Figure 34: Failure mode in the test of 1 in. rigid board

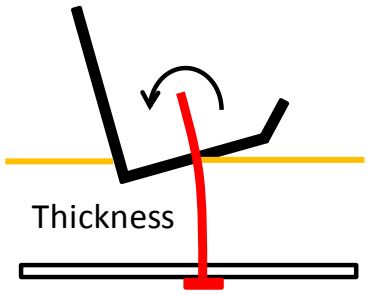

Figure 35: Screw bending due to existing of rigid board

When Z8 specimens with 2 in. of rigid board were tested, the failure mode was a combination of screw bending/fracture and girt yielding. Panel pull-over was prevented by the rigid board insulation's "washer effect" which reinforced the panel and prevented local panel deformation. For a rigid board thickness of 4 in., the only failure mode observed was girt yielding. Screw bending was not observed because of the larger screw diameter employed (#14-1/4).

4.8.2 Zee girts (10 in. deep, 0.060 in. thick)

All Z10 (bare panel and rigid board insulation) girts failed by girt local buckling (Figure 36, 37). Panel pullover or screw bending were not observed because girt cross-section deformation dominated the failure mode. The girt cross-section was locally slender (0.06 in. thick, 10 in. deep), so the cross section itself deformed instead of indenting the rigid board and pulling on the fasteners (see Figure 36). Also, the flange was too thin to develop a concentrated moment on the fastener. A secondary reason for the lack of a panel pullover failure mode was that the failure pressure for the Z10 specimens was lower than that of the Z8 specimens, which means the tensile force on the screws was lower when the girts fail.

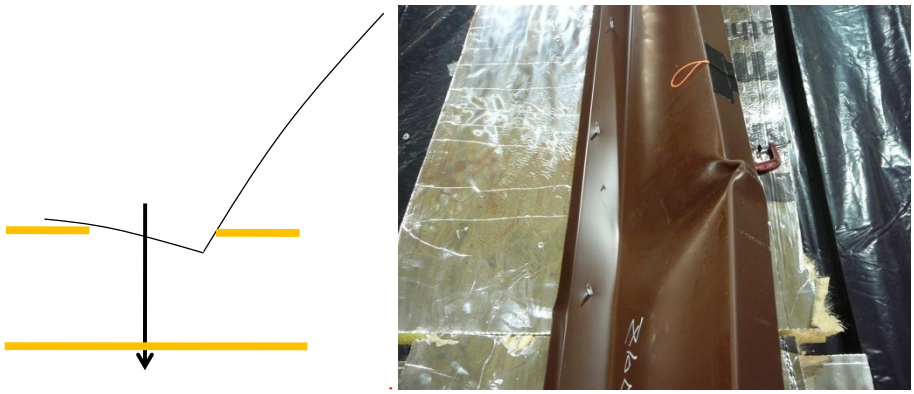

Figure 36: Deformation of slender cross section during the test

Figure 37: Local bucking during the test of slender cross section

4.8.3 Cee (8 in. deep, 0.100 in. thick)

It was observed that Cee section girts rotated more than the Zee girts, primarily because the shear center offset. Because of this significant rotation, severe screw bending was observed, especially because the base metal thickness was thick enough (0.100 in.) to develop a concentrated moment on the fastener.

For the specimens without insulation, the failure mode was similar to the Z8 girts, i.e., panel pull-over. When 1 in. of rigid board insulation was considered, the failure mode was a combination of panel pull-over and screw bending and fracture. Note that this result is different from the Z8 girts - no C8 specimens failed by girt yielding because the screws always broke first.

Panel pull-over was prevented when C8 specimens were constructed with 2 in. of rigid board insulation because of the "washer effect", however the screws still bent and broke. The failure mode became more complex when 4 in. of rigid board was considered, with a combination of bent screws, broken screws, and girt yielding. The failure mode (broken screws or girt yielding) was dependent on the screw location *C*. The broken screw failure mode occurred in the specimens with a small *C*, and the failure mode of girt yielding occurred in specimens with a larger *C*. This trend can be explained in Figure 38, which demonstrates that with a small *C* there is less pressure load (q) to prevent rotation, and therefore the screws break before girt yielding.

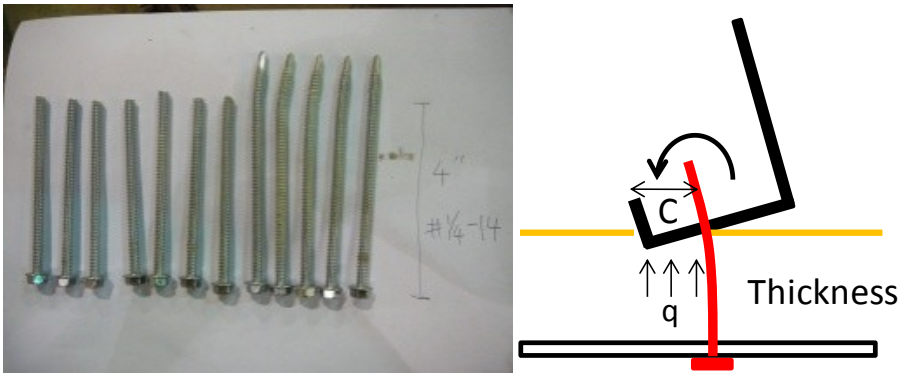

Figure 38: When *C* is small, the resisting moment is small and the screws break

4.8.4 Cee (10 in. deep, 0.060 in. thick)

Similar to the Z10 specimen results, all C10 specimens (bare panel and rigid board insulation) failed by girt local buckling. No panel pullover or bent or broken screws were observed.

4.8.5 Failure mode summary

Specimen failure modes are summarized in Table 9 as a function of rigid board thickness. All 10 in. deep members failed by girt yielding. The rigid board insulation did not influence girt capacity because the slender (0.060 in. thick) cross-section dominated the failure. For the 8 in. deep members (0.100 in. thick), the failure mode changed from panel pull-over to girt yielding when the rigid board thickness was increased. Thick rigid board worked like a washer, reinforcing the panel and preventing panel pull-over. However, at the same time, the rigid board caused bent and broken screws that initiated specimen failure. The C8 girt specimens exhibited severe screw bending because of the cross-section twist created by the shear center offset to the applied load at the fasteners.

Table 9: Failure modes

Rigid Board Thickness, in.	Test Name	Failure Mode
-	Z8D-1	1
	Z8D-2 Z8D-3 Z8DR4-1 Z8DR4-2 Z8B-1 Z8B-2W	2
1	Z8DTH1-1 Z8DTH1-2 Z8BTH1-1 Z8BTH1-2	2,3,4
2	Z8DTH2-1 Z8DTH2-2 Z8BTH2-1 Z8BTH2-2	3,4
4	Z8DTH4-1 Z8DTH4-2 Z8BTH4-1	4

1: Panel bending
2: Screw pull over
3: Screw broken or bent
4: Girt yielding

Rigid Board Thickness, in.	Test Name	Failure Mode
-	Z10D-1 Z10D-2 Z10B-1 Z10B-2	4
1	Z10DTH1-1 Z10DTH1-2 Z10BTH1-1 Z10BTH1-2	4
2	Z10DTH2-1 Z10DTH2-2 Z10BTH2-1 Z10BTH2-2	4
4	Z10DTH4-1 Z10DTH4-2 Z10BTH4-1 Z10BTH4-2	4

1: Panel bending
2: Screw pull over
3: Screw broken or bent
4: Girt yielding

Rigid Board Thickness, in.	Test Name	Failure Mode
-	C8D-1 C8D-2	2
1	C8DTH1-1 C8DTH1-2	2,3
2	C8DTH2-1 C8DTH2-2	3
4	C8DTH4-1 C8DTH4-2	3,(4)

1: Panel bending
2: Screw pull over
3: Screw broken or bent
4: Girt yielding

Rigid Board Thickness, in.	Test Name	Failure Mode
-	C10D-1 C10D-2	4
1	C10DTH1-1 C10DTH1-2	4
2	C10DTH2-1 C10DTH2-2	4
4	C10DTH4-1 C10DTH4-2	4

1: Panel bending
2: Screw pull over
3: Screw broken or bent
4: Girt yielding

4.9 R-Factors

The R-factor is calculated as follow:

$$R = \frac{M_t}{S_e F_y} \tag{16}$$

Where M_t is calculated by Eq. (14) and (15); F_y and S_e are provided in Table 6 and 7. The maximum pressure, P , in Eq. (14), is summarized in Appendix C.

4.9.1 Effect of screw location, C

Rotational restraint and girt capacity are very sensitive to fastener location in the flange. As *C* increases in Figure 39, i.e., as the fastener moves away from the cross-section pivot point on the panel, girt capacity increases. The relationship between girt capacity and *C* is approximately linear for a specific specimen type, however the slope of the line varies with the experimental variables, e.g., insulation thickness and cross-section type. A normalization scheme for the R-factors is implemented in the next section to accommodate a consistent comparison of girt capacity independent of fastener location.

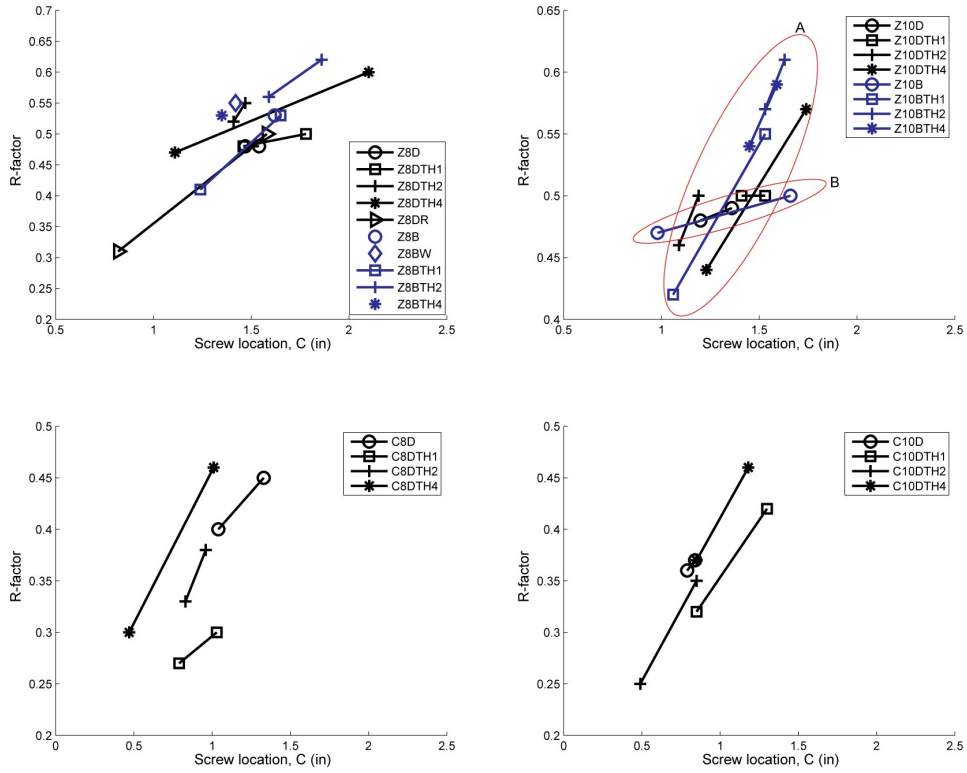

Figure 39: R-factor as a function screw location

4.9.2 Normalization for screw location, C

The current AISI prediction equations assuming that the screw is placed in the middle of flange, and therefore the R-factor is for $C=B/2$, where B is the flange width. However, during the experiments, it was very difficult to guarantee that the screws were always placed in the middle of flange (see Table 8), and even the average C for each group (2 tests) may or may not be close to $B/2$. To compare the results from different groups and the existing AISI S100-07 R-factors, a normalization is performed to shift all the experimentally derived R-factors in this study to $C=B/2$.

As shown in Figure 40, two data points ([$C1$, $R1$], [$C2$, $R2$]) exist for each specimen type (see Table 5, and their average (Ca, Ra) can be easily calculated. The R-factor for $C=B/2$, R^*, is then calculated by $R^*=Ra+k(B/2-Ca)$ as illustrated in the Figure 40. The parameter k is determined in Figure 41 by utilizing the linear relationships between girt capacity and C for each specimen grouping in Figure 39, i.e., for Z8, Z10 (two trend lines A and B), C8, and C10.

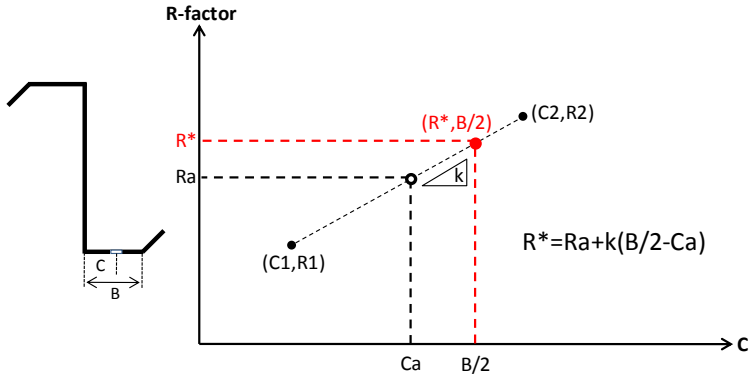

Figure 40: Illustration of correction method

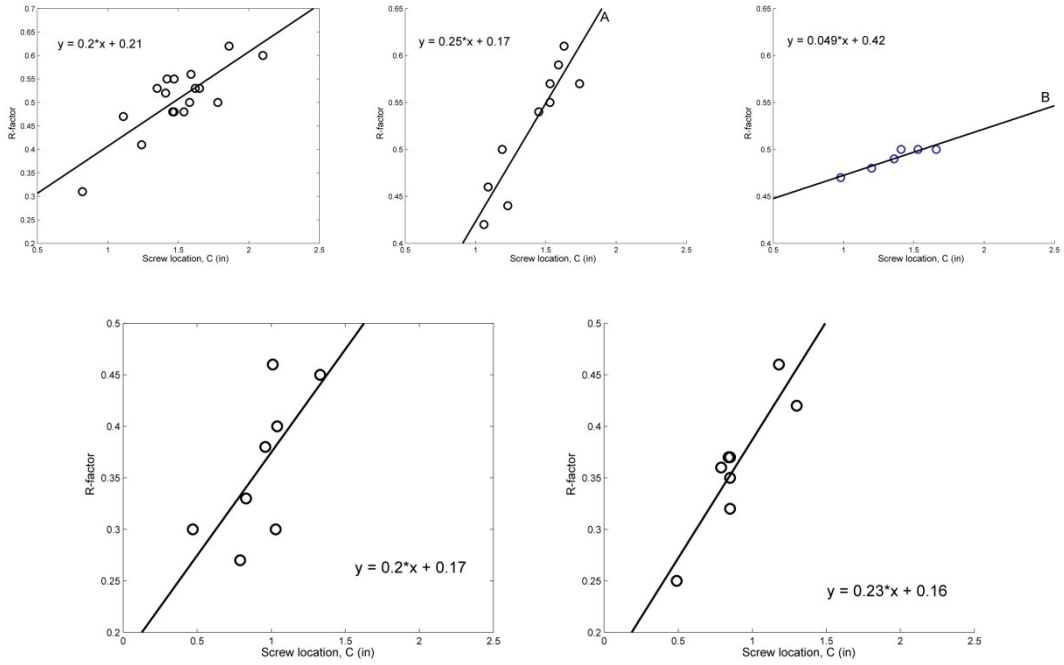

Figure 41: k-factors

4.9.3 Zee sections – bare panel trends

Girt capacity trends for the Zee sections are summarized in Figure 42. (R-factors discussed in this section and following sections has been normalized for *C* using the procedure in Section 4.9.2.) R-factors for the Z8 girts (8 in. deep, 0.1 in. thick) are approximately 25% lower than the current AISI R-factor of 0.65 for 6.5 in. to 8.5 in. deep Zee sections, resulting from the panel pull-over failure mode initiated by a combination of the relatively thin 26 gauge panel and a rigid locally stocky cross-section (see Section 4.8.1). Adding 4 in. of fiberglass insulation resulted in a 4% reduction in the R-factor (Z8DR). The R-factor for test series Z8B is higher than Z8D, because the B panel had a deeper rib and because this panel's higher yield stress increased panel pull-over strength. The R-factor for test series Z8BW (B panel, fastener with washer) is higher than Z8B, because the washer improved panel pullover capacity. Tested Z10 girt (10 in. deep, 0.060 in. thick) R-factors are consistent with the current AISI R-factor of 0.50. Remember, all of these locally slender members failed in local buckling (see Section 4.8.2). This is why girt capacity was not

sensitive to panel type (compare Z10D to Z10B in Figure 42).

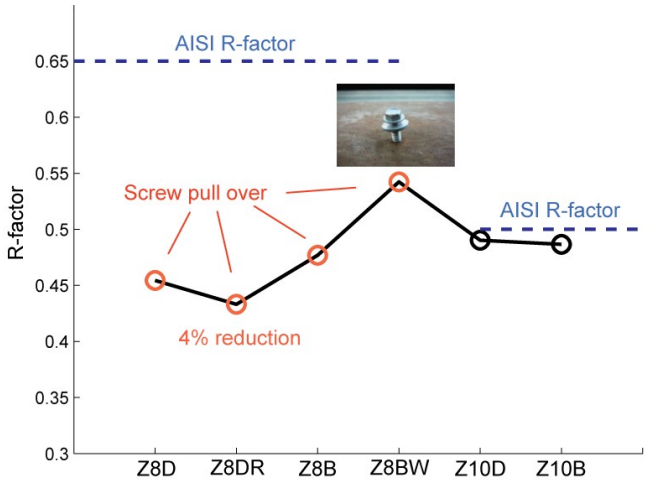

Figure 42: R-factors of the cases of bare panel

4.9.4 Zee Sections - effect of rigid board thickness

The influence of rigid board thickness on R-factor is summarized in Figure 43(a) for the Zee sections test series. For the Z8 girts, the R-factor of bare panel (PANEL in Figure 43) is lower than the current AISI R-factor (0.65) because of panel pull-over. The addition of 1 in. of rigid board (TH1 in Figure 43a) initiates screw bending and is not thick enough to provide the "washer effect" and prevent panel pull-over. An increase to 2 in. of rigid board causes the failure mode to change from panel pullover to girt yielding, and the R-factor in TH2 increases relative to PANEL and TH1. However, although the failure mode for test series TH2 is girt yielding, the R-factor is still lower than 0.65 because of screw bending and the low rotational restraint provided to the girts.

The girt capacity with 4 in. of insulation (TH4) decreases relative to TH2, although higher rotational restraint (thicker board=higher rotational restraint) and a larger screw diameter are provided. A possible reason for this trend is that due to the inconsistency between the principle axis and centroidal axes in Zee section, the cross section shifts laterally during loading (see AISI S100-2007 commentary D3.2.1) as shown in the Fig. 43(a). The 4 in. rigid board may be thick enough to allow this lateral translation. An R-factor reduction in TH4 is not observed in Cee girts where the cross section tends to rotate instead of translating laterally.

The Z10 specimens consistently failed in local buckling. The test series TH1 and TH2 demonstrate a slight increase in R-factor as a function of thickness (thicker board=higher rotational restraint). This trend can be explained by the rotational restraint tests discussed previously (see Figure 20), where the rotational restraint in the first elastic region was demonstrated to be higher than that provided by the bare panel. The decrease in capacity from TH2 to TH4 in Figure 43(a) is again hypothesized to occur because of the Zee section's tendency for lateral translation.

4.9.4 Cee sections - effect of rigid board thickness

All C8 tests (with one exception, TH4) failed because of screw failure or panel pull-over before the girts yielded. In test series TH1, screw bending combined with panel pullover to reduce the R-factor relative to the bare panel case. With 2 in. of rigid board, panel pull-over was avoided, providing higher rotational restraint than 1 in. of rigid board and increasing capacity (compare TH2 to TH1 in Figure 43b). The TH4 test series results in a higher R-factor than TH2 because of the improved rotational restraint from the "washer effect" and because of the larger screw diameter.

Consistent with the Z10 specimens, all C10 specimens failed in local buckling. The R-factor increases slightly as a function of rigid board thickness, because again the rotational restraint increases as a function of board thickness. Overall, cross-section deformation governs and the girts with a slender cross-section are relatively insensitive to rigid board thickness.

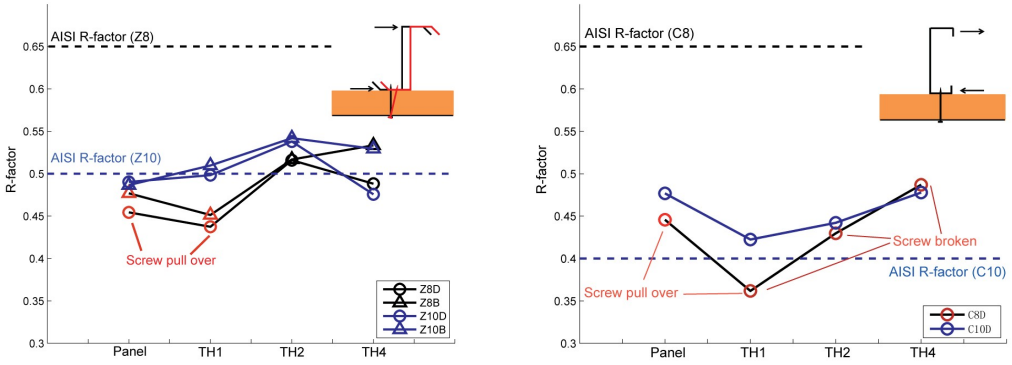

(a) (b)

Figure 43: Influence of rigid board thickness on R-factors for (a) Zees and (b) Cees

5. Conclusions

Rotational restraint tests and vacuum box experiments were conducted to observe and quantify the influence of rigid board insulation on girt capacity in metal building wall systems. Both rotational stiffness and girt capacity (R-factors) were very sensitive to the screw location. In the rotational restraint tests, a trilinear behavior (elastic, plateau and hardening regions) was observed because of the compression stress-strain properties of the insulation. In the initial elastic region, the rigid board provided a slightly higher rotational restraint to girts than just the bare panel. The rigid board provided much less rotational restraint than the bare panel once the insulation's cell walls began to buckle and compress. The higher initial stiffness of XPS compared to Thermax provided more girt rotational restraint, and the rotational restraint increased as a function of board thickness because the insulation reinforced the through-fastened panel at the location of the screw.

Girt capacity was not influenced by rigid board insulation when cross-section slenderness was high (10 in. deep, 0.060 in. thick) because the failure mode was dominated by local buckling in the cross-section. For the locally stocky cross sections (8 in. deep and 0.100 in. thick), panel pull-over was the dominant limit state for tests without insulation, resulting in lower R-factors than those currently specified by AISI S100-07. It is hypothesized that the R-factor for Z8 girts

without insulation could reach 0.65 if panel pullover was prevented.

Adding rigid board prevented panel pullover by preventing local deformation at the fasteners, i.e., the "washer effect". However, the presence of rigid board insulation also resulted in screw bending, especially in the Cee section girts, where cross-section rotation was magnified by the torsion created because of eccentricity of the applied load from the shear center.

Although span length was not an experimental variable, it is hypothesized that the panel pull-over failure mode is sensitive to span length. A longer span is more likely to experience a panel pull-over failure because cross-section rotation is larger at midspan, placing higher tensile forces on the fasteners as they resist the rotation with a force couple, see in Appendix D.

6. Proposed Modifications to AISI S100-07 D6.1

The results presented herein demonstrate that when rigid board insulation (Thermax) is between 2 in. and 4 in., the R-factor is 0.5 for Zee sections and 0.4 for Cee sections, independent of web depth. If the rigid board insulation is thinner than 2 in., the R-factor could be reduced by the panel pullover limit state depending upon the panel thickness. There is currently no provision in AISI S100-07 D6.1 addressing the panel pullover limit state, and therefore rigid board thicknesses of 1 in. or less should be avoided, and even for the case without insulation, more research is needed to remedy this apparent inconsistency in the current specification. Proposed specification language is provided in Appendix E.

7. Future Work

The results from this study have demonstrated that there are at least four separate limit states for through-fastened metal building wall systems with or without rigid board insulation (Figure 44) – panel bending, screw pullover, screw bending/fracture, and girt failure (either yielding or local buckling). Which limit state controls is dependent upon several variables, including cross-section slenderness, span length, and girt capacity. For a slender cross-section, cross-section deformation dominates and the large tensile forces needed to develop a panel pull-over failure cannot be achieved. Longer spans results in larger girt rotations that can cause panel pullover (see Appendix D). Panel thickness and yield stress also affect the panel pull-over limit state.

(screw pull over) (Screw bending/broken)

(Girt yielding)

Figure 44: Failure modes observed after tests

In previous research by Fisher (1996), which serves as the basis for the current R-factors in AISI S100-07 D6.1, 4 tests failed by panel pull-over, and 25 tests by girt failure. Note in Figure 45 that most of the cross-sections selected in Fisher's study were locally slender, and therefore the panel pull-over limit state was not strongly identified as a possible limit state. In the four tests that did fail by panel pullover, the cross-section was locally stocky, and the R-factor was lower than that of a girt failure, which is consistent with the trends observed in this research.

A key component to the development of a limit state approach will be the use of the AISI Direct Strength Method. A proposed strength prediction method for the girt limit state is described in Appendix A. More research is needed to validate an approach for predicting the fastener tensile force and relating the demand to existing AISI pull-over prediction equations. Provisions for treating the screw bending-tension interaction observed in this research are also needed.

Test No.	Member Type	Member Depth (in.)	Member Length (ft.)	Member Thick. (in.)	Tested Moment Capacity (ft.-kips)	Calculated Nominal Moment (ft. kips)	R	Failure Mode	Slenderness
1	Z	8.0	19.17	0.1023	9.23	15.78	0.59	1,2	78
2	Z	8.0	19.17	0.1023	8.98	15.74	0.57	2	78
3I	Z	8.0	19.17	0.1028	8.73	15.76	0.55	2	78
4I	Z	8.0	19.17	0.1026	7.70	15.88	0.49	2	78
5			19.17	0.0605	3.94	6.15	0.64	2	107
6			19.17	0.0610	3.64	6.25	0.58	2	107
7			19.17	0.0600	4.53	9.47	0.48	2,3,4	133
8			19.17	0.0704	5.73	10.83	0.53	2,3,4	114
9			19.17	0.0656	6.12	12.98	0.47	2,3	145
10	Z	9.5	19.17	0.0738		15.18	0.54	2	129
11	Z	11.5	19.17	0.0825		20.22	0.47	3	139
12	C	6.5	19.17	0.0598		6.43	0.64	2	109
13	C	6.5	19.17	0.0599		6.50	0.67	2	109
14	C	8.0	18.75	0.0602		8.40	0.49	2	133
15	C	8.0	18.75	0.0760	7.30		0.68	2	105
16	Z	6.5	24.17	0.0827	5.56	8.93	0.62	2	79
17	C	6.5	24.17	0.0821	7.80	9.94	0.79	2	79
18	Z	8.0	24.17	0.0807	7.76		0.58	2	99
19	Z	8.0	24.17	0.0814	7.44	12.57	0.59	2	98
20	Z	8.0	24.17	0.0819	8.25	13.17	0.63	2	98
21I	Z	8.0	24.17	0.0820	7.27	11.64	0.62	2	98
22I	Z	8.0	24.17	0.0812	7.76	13.08	0.59	2	99
23I	Z	8.0	24.17	0.0818	7.11	13.33	0.53	2	98
24I			24.17	0.0814	7.27	13.19	0.55	2	98
25I			24.17	0.0807	7.28	13.02	0.56	2	99
26			29.17	0.1034	7.80	16.03	0.49	1	77
27			29.17	0.1178	11.74	22.28	0.53	1	81
28	C	8.0	29.17	0.1015	9.11	13.38	0.68	1	79
29	C	9.5	29.17	0.0895	10.14	17.72	0.57	1	106

Shorter span

Lower SeFy

Longer span

slender

slender

Failure Modes
1 = Screw pull through deck
2 = Local buckling of member
3 = Deck failure
4 = Purlin had wavy stiffener lips

Figure 45: Tests in previous research (Fisher 1996)

References

AISI (2007). AISI S100-07 North American Specification for the Design of Cold-Formed Steel Structural Members. American Iron and Steel Institute, Washington, D.C.

AISI (2008). AISI Manual for Cold-Formed Steel Design. American Iron and Steel Institute, Washington, D.C.

Fisher, JM (1996). "Uplift Capacity of Simple Span Cee and Zee Members with Through-Fastened Roof Panels", Report for Metal Building Manufacturers Association.

Lucas RM, Al-Bermani GA, Kitipornchai S. (1997) "Modelling of Cold-Formed Purlin-Sheeting Systems. Part 1: Full Model", *Thin-Walled Structures*, 27(3), 223-243.

LaBoube RA (1986). "Roof Panel to Purlin Connections: Rotational Restraint Factor", *Proceedings of the IABSE Colloquium on Thin-Walled Metal Structures in Buildings,* Stockholm, Sweden.

Laboube, RA (1983). "Laterally Unsupported Purlins Subjected to Uplift", Report for Metal Building Manufacturers Association.

LaBoube, RA, and Thompson, MB (1982). "Static Load Tests of Braced Purlins Subjected to Uplift load", MRI Report No. 7485-6.

Perry, D, Golovin, M, Montague, D, LaBoube, RA, and Wilson L (1987). "Continuous Purlin Uplift Tests", Report for Metal Building Manufacturers Association.

Pekoz, T, and Soroushian, P. (1982). "Behavior of C- and Z-Purlins under Wind uplift", Proceedings of the Sixth International Specialty Conference on Cold-Formed Steel Structures, November.

Rousch CJ, Hancock GJ (1997). "Comparison of tests of bridged and unbridged purlins with a non-linear analysis model", *Journal of Constructional Steel Research*, 41(2-3), 197-220.

Schafer BW, Sangree RH, Guan Y. (2007). "Experiments on Rotational Restraint of Sheathing", final Report for American Iron and Steel Institute-Committee on Framing Standards.

Schafer BW, Adany S. (2006). "Buckling analysis of cold-formed steel members using CUFSM: conventional and constrained finite strip methods", *Eighteenth International Specialty Conference on Cold-Formed Steel Structures,* Orlando, FL, 2006.

Vieira, Jr., LCM, Malite, M, and Schafer, BW. (2010). "Simplified models for cross-section stress demands on C-section purlins in uplift", Thin-walled Structures, 48(1)33-41.

Winter, G, Lansing, W, and McCalley, RB (1950). "Performance of Laterally Loaded Channel Beams", Performance of thin-walled steel structures, Cornell University, Engineering Experiment Station, Reprint No.33.

Appendix A – Direct Strength Method - Through-Fastened Girts

EUROSTEEL 2011, August 31 - September 2, 2011, Budapest, Hungary

FLEXURAL CAPACITY PREDICTION OF METAL WALL GIRTS
Using the Direct Strength Method

Tian Gao [a], Cristopher D. Moen [b]

[a,b] The Charles E. Via, Jr. Department of Civil and Environmental Engineering, Virginia Tech, USA

INTRODUCTION

The critical load case for cold-formed steel wall girts in pre-manufactured metal buildings is suction caused by wind, which places a girt's unbraced flange in compression as it spans between building frames. The resulting failure mode is restrained lateral-torsional buckling, where rotational restraint is provided to the girt by through-fastened exterior metal panels (*Fig.1*).

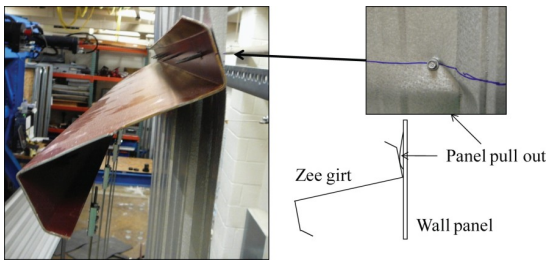

Fig. 1. Rotational restraint provided by metal panels

Strength prediction of through-fastened girts is challenging. For Zee section girts, bending occurs about the principal axes, resulting in a complex stress distribution through the member depth. For Cee and Zee section girts, the fastener load is applied offset to the shear center, resulting in longitudinal warping torsion stresses that combine with flexural stresses [1, 2]. Both Cee and Zee section girts tend to roll upon load application, resulting in a longitudinal stress distribution that changes with loading magnitude. This is why girt flexural capacity is typically predicted with experimentally derived R-factors, e.g., AISI S100-07 D6.1 [3].
Experiments have demonstrated that through-fastened girt flexural capacity is sensitive to web height, flange width, girt thickness [4, 5, 6], metal panel thickness [7], and fastener location in the girt flange [8]. In this paper, the relationship between these parameters and girt capacity are evaluated with a new girt flexural strength prediction method employing the AISI Direct Strength Method, which in the future may provide an alternative to the current R-factor approach. The new method is employed to calculate the capacity of 57 Zee section and 85 Cee section girts. The new method employs a recently derived mechanics-based model for approximating panel-to-girt rotational restraint that accounts for girt cross-section dimensions and through-fastened metal panel profile and thickness [8]. Predicted capacities are compared to existing experimentally derived R-factors, and parameter studies demonstrate trends in girt capacity with cross-section dimensions.

1 GIRT CAPACITY PREDICTION WITH THE DIRECT STRENGTH METHOD (DSM)

The proposed DSM girt capacity prediction procedure is summarized in *Fig. 2*. For a given cross-section with the through-fastened flange placed in tension and the free flange placed in compression, the tension flange-web intersection is assumed to be partially restrained in rotation by a spring and fully restrained in *x*-direction translation. The cross-section and spring with rotational stiffness, k_ϕ, are input into the finite strip analysis program CUFSM [9]. The critical elastic local ($M_{cr\ell}$), distortional (M_{crd}) and lateral-torsional (M_{cre}) buckling moments are then used to determine the nominal flexural strength, M_n, with DSM. The R-factor is also calculated for comparison,

determined as the ratio of M_n from DSM to S_eF_y, where S_e and F_y are the effective section modulus and member yield stress.

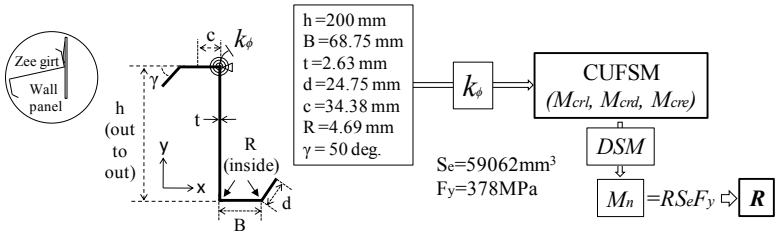

Fig. 2. R-factor prediction procedure

2 PANEL-TO-GIRT ROTATIONAL RESTRAINT

The panel-to-girt rotational restraint, k_ϕ (Nmm/rad/mm), is defined as the ratio of moment (Nmm/mm) applied at the corner of flange and web to the rotation (rad) of the web as shown in *Fig. 3*. The spring is located at the corner of the cross-section to capture the flange bending effect [8] in the finite strip analysis.

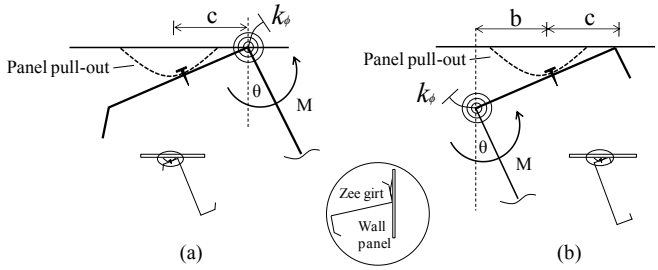

Fig. 3. Rotational restraint k_ϕ in a (a) Zee (b) Cee

For a member with Zee and Cee cross-section, k_ϕ is calculated in *Eqs.(1)*

$$k_{\phi-z} = \frac{1}{\frac{1}{kc^2} + \frac{c}{3EI}}, \quad k_{\phi-c} = \frac{1}{\frac{1}{kc^2} + \frac{\frac{b^2c}{2} + bc^2 + \frac{c^3}{3}}{EIc^2}} \tag{1}$$

where k is the panel pull-out stiffness (N/mm/mm) calculated empirically as k=4.15$c^{-0.4}$ from a linear elastic finite element analysis (*Fig.4*) documented in [8]; EI is the panel bending rigidity [E=203GPa, I=t^3/12 (mm^4/mm), t=member thickness (mm)]; c is the distance between the centerline of the screw and the section pivot point, i.e., the corner of web and flange in a Zee section and the corner of lip and flange in a Cee section; and b is the distance between the screw and the corner of web and flange in a Cee section (See *Fig.3*).

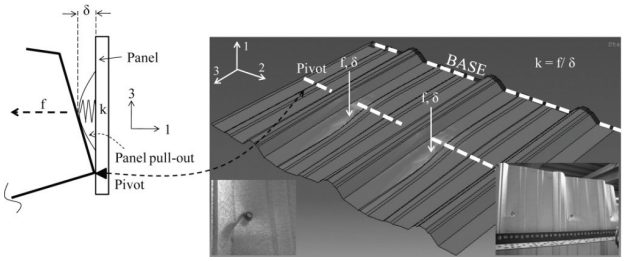

Fig. 4. FE derived pull-out stiffness, $k=f/\delta$ divided by fastener spacing

3 GIRT CAPACITY PARAMETER STUDIES

A prediction example of a Zee section is shown in *Fig.5*, and the member properties are shown in *Fig.2*. A rotational spring stiffness k_ϕ = 1191 Nmm/rad/mm is calculated with *Eqs.(1)* and then the procedures in *Fig.2* are implemented, resulting in an R-factor of 0.67. In CUFSM, the reference stress is applied at the cross-section as unrestrained bending as shown in *Fig.5*. The change in stress distribution from cross-section rotation during loading is ignored in this study, however it is a focus of ongoing research. Also note that when the rotational spring is added, global buckling occurs at a finite half-wavelength instead of being a function of physical length.

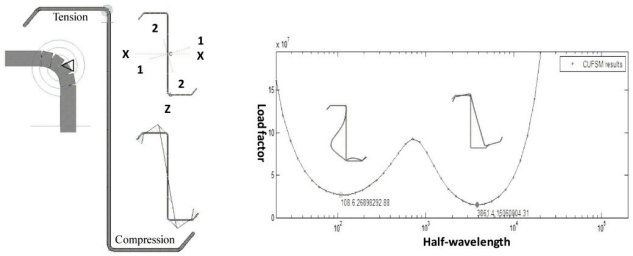

Fig. 5. Prediction example with finite strip method (CUFSM)

3.1 Cross-sections in AISI manual and limits in AISI S100-07 Section D6.1

Using the prediction method described in Section 1, R-factors of 57 Zee and 85 Cee sections (*Fig.6*) from the AISI Design Manual [10] are calculated, where F_y is 378 MPa, E is 203 GPa, and Poisson's ratio is 0.30. For each cross section, S_e is given in the AISI Design Manual [10].

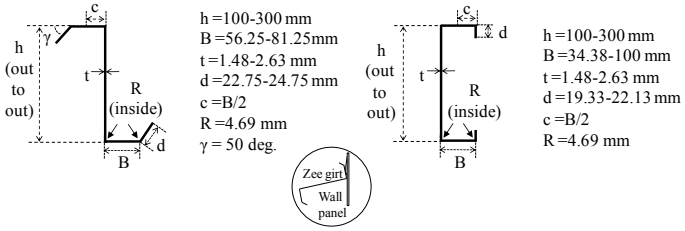

Fig. 6. Cross-sections considered, identical top and bottom flanges assumed

To use the R-factor approach in AISI S100-07 Section D6.1, the girt cross-section must meet the limits in *Eqs.(2)*

$$h \le 292(mm),\ 60 \le h/t \le 170,\ 2.8 \le h/B \le 4.5,\ 16 \le B_f/t \le 43 \quad (B_f = B - 2t - 2R), \tag{2}$$

where B_f is the flat flange width. If variables fall outside these limits, full-scale testing is required.

4 RESULTS AND DISCUSSION

4.1 Influence of member depth *h* on R-factors

Predicted R-factors (x: out of limits of *Eqs.(2)*; o: in limits) are plotted in *Fig.7* as a function of web depth *h* along with the R-factors (solid line) in AISI S100-07 D6.1. Generally, for both Zee and Cee sections, R-factor decreases as a function of web depth. On average, predicted Zee section girt capacity shows good agreement with AISI S100-07, while the prediction of Cee section is higher than AISI S100-07. It is hypothesized that DSM Cee girt capacity is higher than AISI S100-07 predictions because warping torsion longitudinal stresses from the offset of the flange loading point to the shear center [1, 2] are not included in this study.

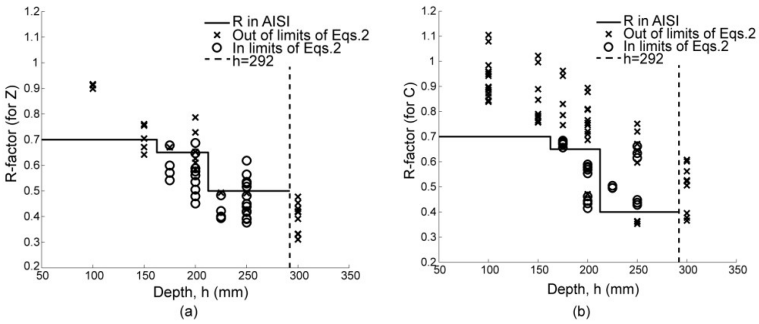

Fig. 7. Predicted R-factors of (a) Zee and (b) Cee sections as a function of web depth

The R-factor increases with increasing member thickness and flange width as shown in *Fig.8*. R-factors for Zee and Cee cross-sections having the same web depth (*h*=200mm) but different thickness (*t*) and flange width (*B*) are plotted in *Fig.8*. At the web depth considered in *Fig.8* (200mm), the R-factor can vary from 0.45 to 0.80 for Zee sections and 0.40 to 0.90 for Cee sections.

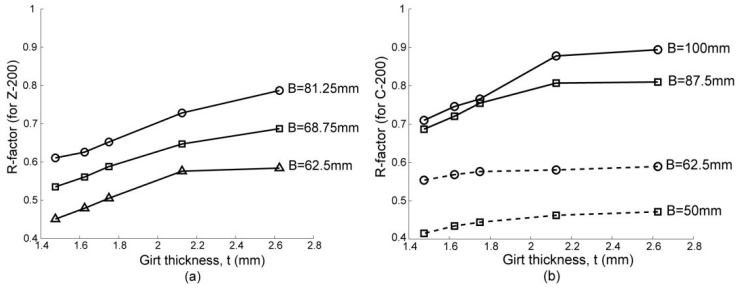

Fig. 8. Predicted R-factors of *h*=200mm (a) Zee and (b) Cee sections with different *t* and *B*

4.2 Influence of *h/t* on R-factors

The R-factors are plotted as a function of *h/t* in *Fig.9*. Generally, the R-factor decreases with increasing *h/t* for both Zee and Cee sections. For Zee sections in this study, the decreasing rate of the R-factor levels off at *h/t* of 100. The wide variation in *Fig.9* is caused by cross-sections with different flange widths (wider flanges have a higher R-factor). See *Fig.8* for the correlation between R-factor and *h/t* for a specific flange width.

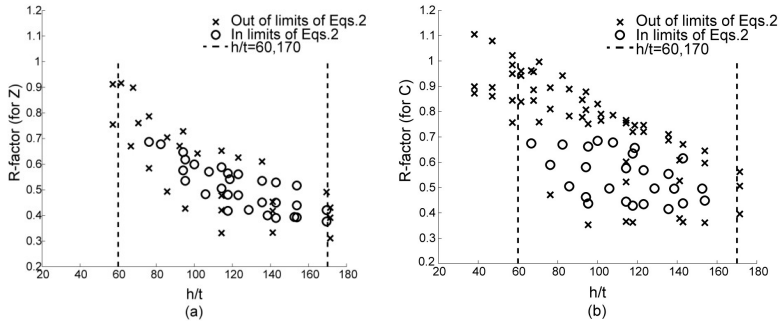

Fig. 9. Predicted R-factors of (a) Zee and (b) Cee sections as a function of *h/t*

4.3 Influence of *h/B* on the R-factors

A clear correlation between *h/B* and R-factor is shown in *Fig. 10*. The R-factor decreases as *h/B* increases. Prediction variability is caused by differences in member depth and thickness. See the effects of member depth and thickness on R-factor in *Fig. 7* and *Fig. 8* respectively.

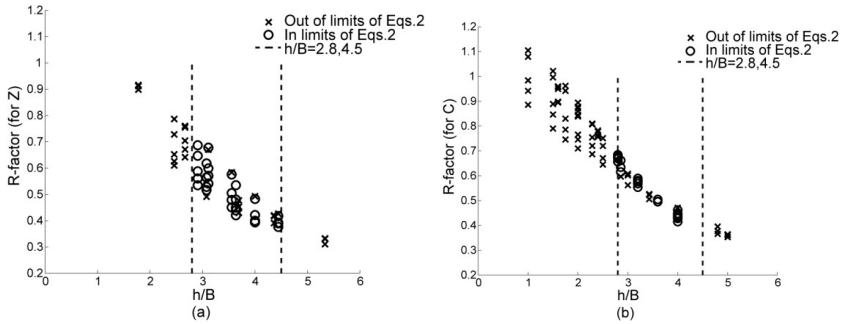

Fig. 10. Predicted R-factors of (a) Zee and (b) Cee sections as a function of *h/B*

4.4 Influence of screw location *c* on the R-factors

In both AISI S100-07 D6.1 and the proposed prediction procedure herein, the screw is located at the middle of flange (*c*=*B*/2, see *Fig.6*). However, in construction, the screw location may vary. The sensitivity of R-factor to *c* is shown in *Fig. 11*. The R-factor increases as a function of *c/B* and can vary from 0.30 to 0.90 for the same girt and panel.

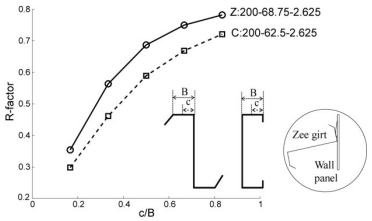

Fig. 11. Predicted R-factors of Zee and Cee sections as a function of screw location

5 CONCLUSIONS AND FUTURE WORK

In this study, a girt flexural strength (R-factor) prediction method using DSM is proposed, and the R-factors of Zee and Cee members in AISI Design Manual were evaluated. The predicted R-factors in Zee members show good agreement with those predicted by AISI S100-07 D6.1, while the predicted R-factors in Cee members are higher than AISI S100-07 D6.1, at least in part because the torsional stress due to the shear center offset in member was not considered in this study. The DSM prediction method demonstrates the sensitivity of the R-factor (girt capacity) to member depth, member thickness, flange width, and screw location for both Zee and Cee members.

6 ACKNOWLEDGMENTS

The authors are grateful for the support provided by the Metal Building Manufacturers Association (MBMA) and American Iron and Steel Institute (AISI) on this research project.

REFERENCES

[1] Winter, G, Lansing, W, and McCalley, RB, "Performance of Laterally Loaded Channel Beams", *Performance of thin-walled steel structures*, Cornell University, Engineering Experiment Station, Reprint No.33, 1950.

[2] Vieira, Jr., LCM, Malite, M, and Schafer, BW, "Simplified models for cross-section stress demands on C-section purlins in uplift", *Thin-walled Structures*, 48(1)33-41, 2010.

[3] AISI-S100 North American Specification for the Design of Cold-Formed Steel Structural Members. American Iron and Steel Institute, Washington, D.C., 2007.

[4] Laboube, RA, "Laterally Unsupported Purlins Subjected to Uplift", Report for Metal Building Manufacturers Association, 1983.

[5] Perry, D, Golovin, M, Montague, D, LaBoube, RA, and Wilson L, "Continuous Purlin Uplift Tests", Report for Metal Building Manufacturers Association, 1987.

[6] Fisher, JM, "Uplift Capacity of Simple Span Cee and Zee Members with Through-Fastened Roof Panels", Report for Metal Building Manufacturers Association, 1997.

[7] LaBoube, RA, "Roof Panel to Purlin Connections: Rotational Restraint Factor", *Proceedings of the IABSE Colloquium on Thin-Walled Metal Structures in Buildings*, Stockholm, Sweden, 1986.

[8] Gao, T, and Moen, CD, "A prediction model for girt-panel interaction in metal building wall systems", *The 6th International Conference on Thin Walled Structures*, Timisoara, Romania, 2011.

[9] Schafer, BW, and Adany, S, "Buckling analysis of cold-formed steel members using CUFSM: conventional and constrained finite strip methods", *Eighteenth International Specialty Conference on Cold-Formed Steel Structures*, Orlando, FL, 2006.

[10] AISI Manual for Cold-Formed Steel Design. American Iron and Steel Institute, Wash, D.C., 2008.

[11] Pekoz, T, and Soroushian, P, "Behavior of C- and Z-Purlins under Wind uplift", *Proceedings of the Sixth International Specialty Conference on Cold-Formed Steel Structures*, November, 1982.

[12] LaBoube, RA, and Thompson, MB, "Static Load Tests of Braced Purlins Subjected to Uplift load", MRI Report No. 7485-6, August, 1982.

Appendix B – Experimental Setup

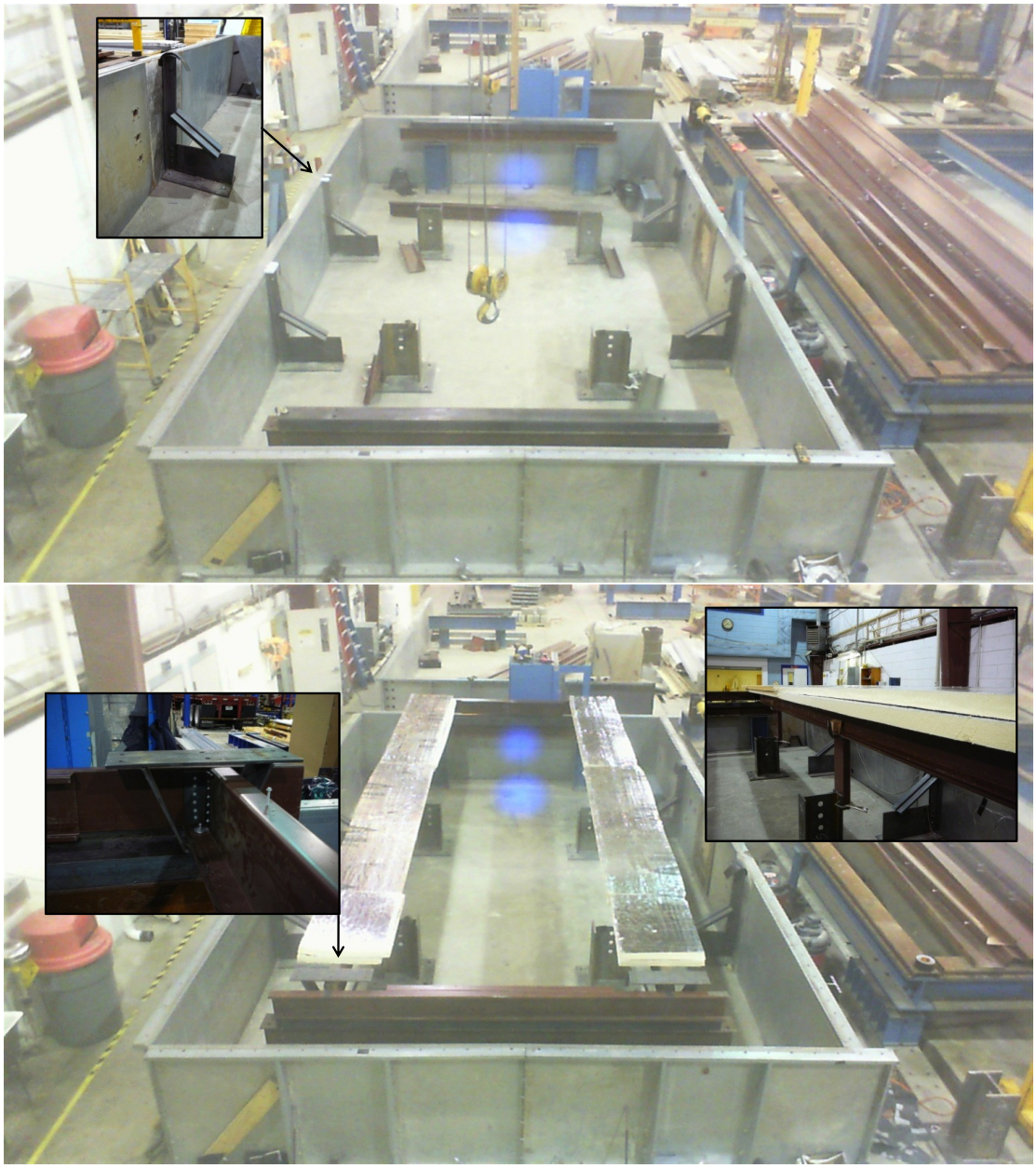

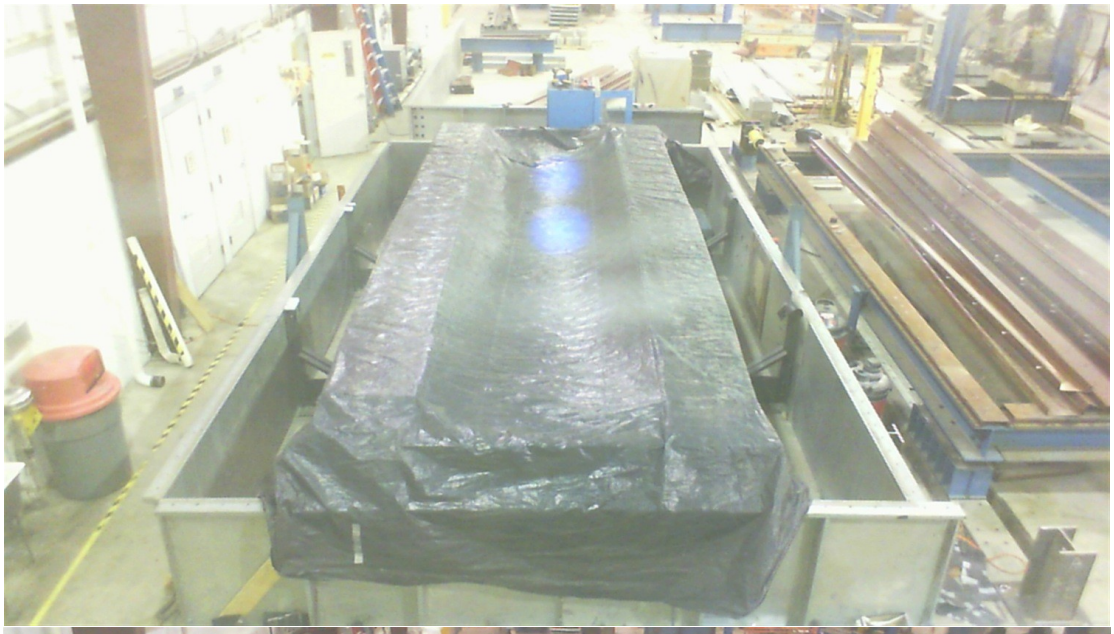

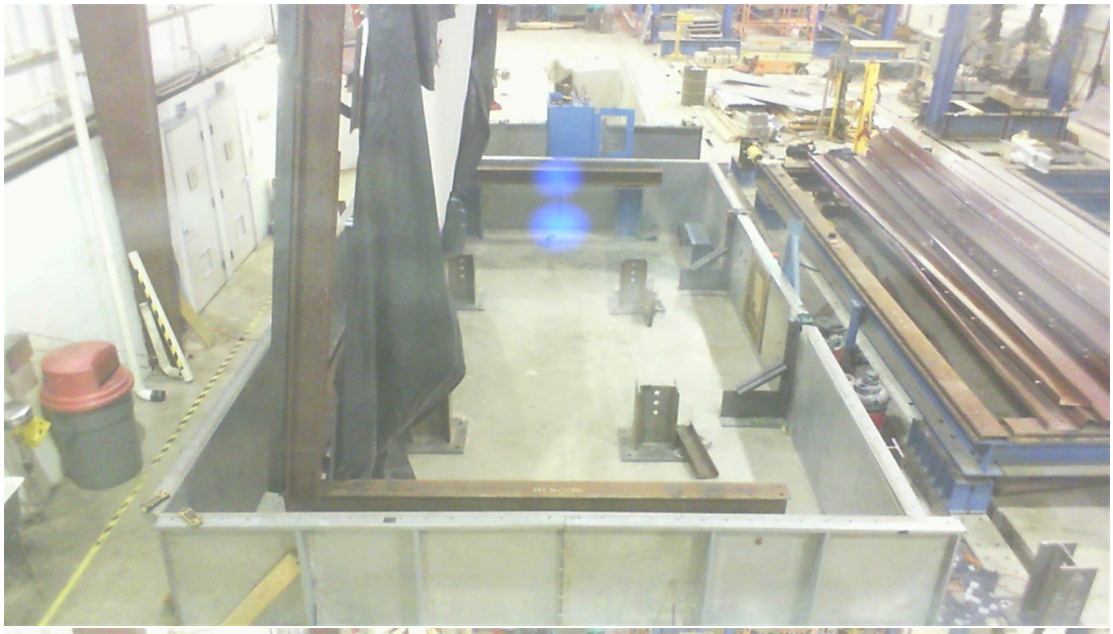

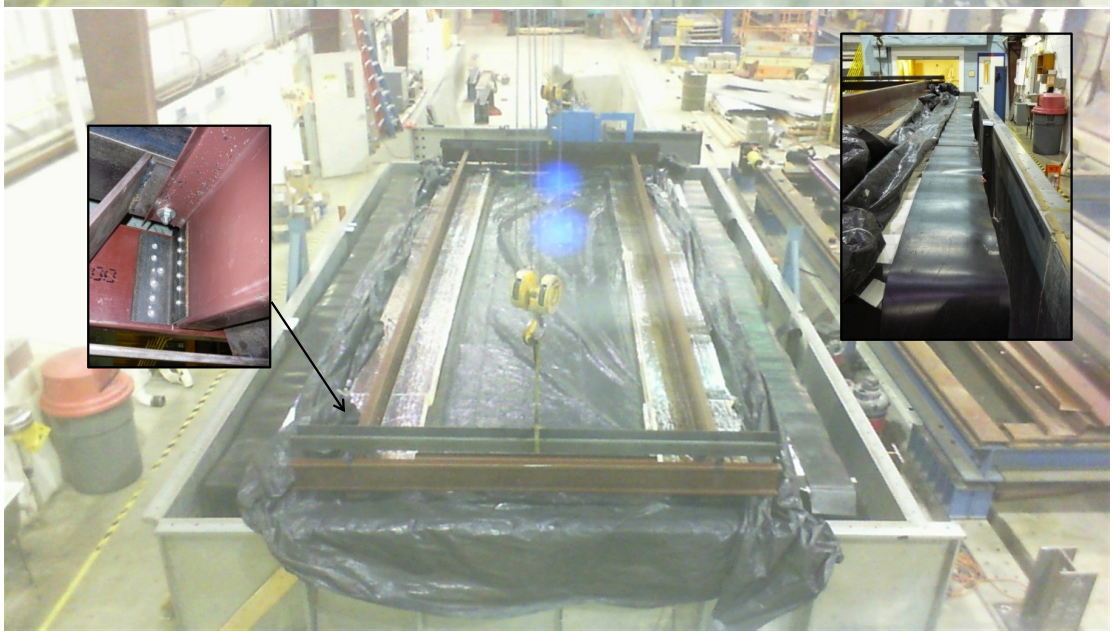

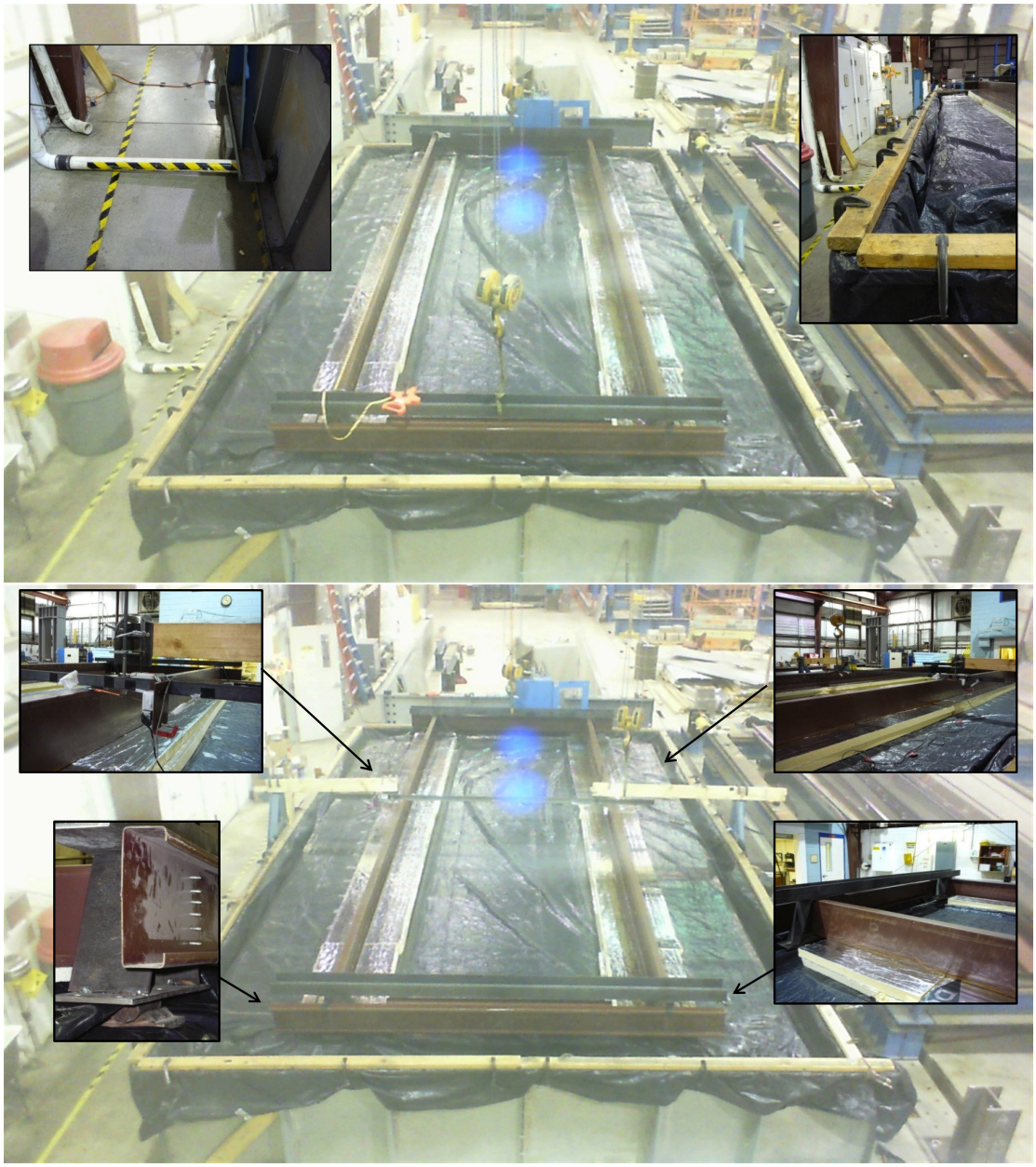

Appendix C – Summary Table

#	Test name	Girt	Web in.	Panel	Insulation	Thickness in.	Pressure, P psf	S_e in^3	F_y ksi	M_t k-in.	R	C in.	Failure Mode
1	Z8D-1	Zee	8	D	None	0							1
2	Z8D-2				None	0	16.41	3.57	60.97	105.56	0.48	1.54	2
3	Z8D-3				None	0	15.82	3.50	60.18	101.93	0.48	1.47	2
4	Z8DR4-1				R13	4	16.85	3.51	62.05	108.25	0.50	1.58	2
5	Z8DR4-2				R13	4	9.88	3.55	60.60	65.61	0.31	0.82	2
6	Z8DTH1-1				Thermax	1	16.08	3.50	62.05	103.53	0.48	1.46	2,3,4
7	Z8DTH1-2				Thermax	1	17.08	3.59	60.61	109.62	0.50	1.78	2,3,4
8	Z8DTH2-1				Thermax	2	17.74	3.39	61.38	113.68	0.55	1.47	3,4
9	Z8DTH2-2				Thermax	2	16.74	3.36	61.71	107.59	0.52	1.41	3,4
10	Z8DTH4-1				Thermax	4	15.08	3.32	61.89	97.44	0.47	1.11	4
11	Z8DTH4-2				Thermax	4	20.06	3.49	61.00	127.89	0.60	2.10	4
12	Z8B-1			B	None	0	18.07	3.47	62.76	115.71	0.53	1.62	2
13	Z8B-2W				None	0	18.65	3.56	60.58	119.22	0.55	1.42	2
14	Z8BTH1-1				Thermax	1	18.07	3.56	61.03	115.71	0.53	1.65	2,3,4
15	Z8BTH1-2				Thermax	1	13.67	3.59	60.98	88.76	0.41	1.24	2,3,4
16	Z8BTH2-1				Thermax	2	21.06	3.49	61.53	133.98	0.62	1.86	3,4
17	Z8BTH2-2				Thermax	2	19.07	3.54	61.50	121.80	0.56	1.59	3,4
18	Z8BTH4-1				Thermax	4	17.75	3.51	61.01	113.74	0.53	1.35	4
19	Z10D-1		10	D	None	0	9.63	2.19	58.49	62.70	0.49	1.36	4
20	Z10D-2				None	0	9.48	2.21	58.09	61.78	0.48	1.20	4
21	Z10DTH1-1				Thermax	1	9.78	2.16	58.53	63.61	0.50	1.53	4
22	Z10DTH1-2				Thermax	1	9.68	2.12	59.30	63.00	0.50	1.41	4
23	Z10DTH2-1				Thermax	2	8.98	2.18	58.80	58.74	0.46	1.09	4
24	Z10DTH2-2				Thermax	2	9.68	2.18	58.35	63.00	0.50	1.19	4
25	Z10DTH4-1				Thermax	4	11.67	2.30	57.62	75.19	0.57	1.74	4
26	Z10DTH4-2				Thermax	4	8.88	2.23	59.35	58.13	0.44	1.23	4
27	Z10B-1			B	None	0	9.18	2.20	58.21	59.96	0.47	0.98	4
28	Z10B-2				None	0	9.98	2.24	57.88	64.83	0.50	1.66	4
29	Z10BTH1-1				Thermax	1	8.58	2.27	58.35	56.30	0.42	1.06	4
30	Z10BTH1-2				Thermax	1	10.97	2.23	57.69	70.92	0.55	1.53	4
31	Z10BTH2-1				Thermax	2	11.67	2.12	57.73	75.19	0.61	1.63	4
32	Z10BTH2-2				Thermax	2	10.97	2.13	58.35	70.92	0.57	1.53	4
33	Z10BTH4-1				Thermax	4	10.67	2.08	56.29	69.09	0.59	1.45	4
34	Z10BTH4-2				Thermax	4	11.27	2.27	59.38	72.75	0.54	1.59	4
35	C8D-1	Cee	8	D	None	0	16.65	3.11	75.73	107.04	0.45	1.33	2
36	C8D-2				None	0	14.46	3.11	75.34	93.63	0.40	1.04	2
37	C8DTH1-1				Thermax	1	9.68	3.11	76.16	64.39	0.27	0.79	2,3
38	C8DTH1-2				Thermax	1	10.68	3.04	76.31	70.48	0.30	1.03	2,3
39	C8DTH2-1				Thermax	2	11.67	3.11	74.52	76.58	0.33	0.83	3
40	C8DTH2-2				Thermax	2	13.67	3.07	76.95	88.76	0.38	0.96	3
41	C8DTH4-1				Thermax	4	17.15	3.08	78.44	110.08	0.46	1.01	4
42	C8DTH4-2				Thermax	4	11.18	3.07	79.38	73.53	0.30	0.47	3
43	C10D-1		10		None	0	6.89	2.06	61.30	45.94	0.36	0.79	4
44	C10D-2				None	0	6.89	2.07	60.06	45.94	0.37	1.10	4
45	C10DTH1-1				Thermax	1	5.99	2.09	59.57	40.46	0.32	0.85	4
46	C10DTH1-2				Thermax	1	7.89	2.08	59.42	52.04	0.42	1.30	4
47	C10DTH2-1				Thermax	2	6.29	2.04	59.93	42.29	0.35	0.85	4
48	C10DTH2-2				Thermax	2	4.50	2.08	59.85	31.32	0.25	0.49	4
49	C10DTH4-1				Thermax	4	6.69	2.03	60.42	44.73	0.37	0.85	4
50	C10DTH4-2				Thermax	4	8.78	2.07	59.94	57.52	0.46	1.18	4

Failure Mode
1: Panel bending
2: Screw pull over
3: Screw broken or bent
4: Girt yielding

Member Thickness
8 in. web: 0.1 in.
10 in. web: 0.06 in

Panel Thickness=26 Ga.
Panel Rib Depth:
D: 1-1/8 in.
B: 1-1/4 in.

Panel Yielding Stress:
D: 50 ksi
B: 80 ksi

Screw: #12 or 1/4-#14 (only for 4 in. board test), No washer except for test #13

All Span=24.5 ft

Appendix D – Rotational Restraint as a Function of Span Length

The vertical loading *Q* introduces a couple of horizontal loading *P* as shown in Figure D-1 due to the anti-symmetry (Zee) and shear center offset (Cee). Notice that *C* is a constant depending on the cross section dimensions. (More details see AISI 2007 Commentary D3.2.1)

$$P = QC \tag{D1}$$

$$C = I_{xy} / 2I_x \quad \text{(for Zee section)} \tag{D2}$$

$$C = e/d \quad \text{(for Cee section)} \tag{D3}$$

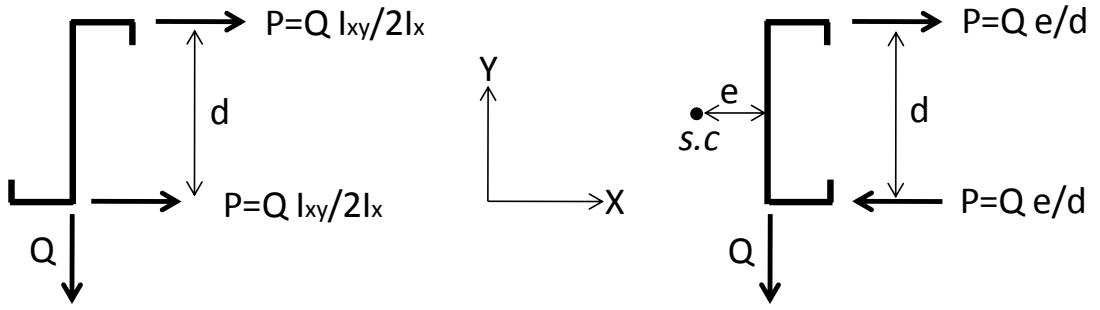

Figure D-1. Horizontal loading introduced by the vertical loading due to the anti-symmetry (Zee) and shear center offset (Cee)

Based on Winter's model, the cross section with a slender web, such as Zee or Cee, can be decoupled into two parts: top flange plus proportion of web, and bottom flange plus proportion of web. Each part is treated as a simply supported beam as shown in Figure D-2, and the horizontal displacement at midspan, Δ, is calculated as:

$$\Delta = \frac{5PL^4}{384EI} \tag{D4}$$

Used as girts or purlin, a flange (bottom flange in Figure D-2) is through fastened to the wall or roof panels, and fully restraint horizontally.

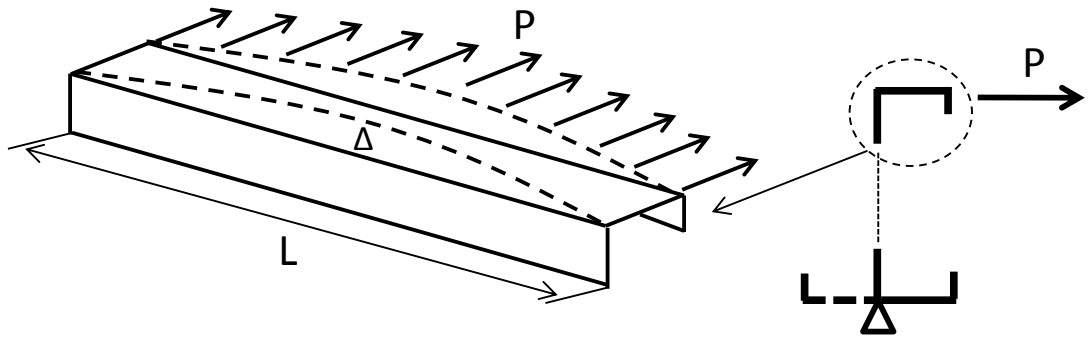

Figure D-2. Decoupling the cross section (Winter's model)

The bending moment, M, around X-axis in Figure D-1 at the midspan can be calculated as:

$$M = \frac{QL^2}{8} \tag{D5}$$

where L is the span length, and Q is the vertical loading. Combining Eq. (D1), (D4) and (D5),

$$\Delta = \frac{40MC}{384EI} L^2 \tag{D6}$$

At the midspan moment, M, used to determine the flexural capacity, the same cross-section ($40MC/384EI$=constant) with different span lengths L_1 and L_2 gives $\Delta_1/\Delta_2=L_1^2/L_2^2$. Δ actually is representing the rotation of the cross section, since the bottom flange is fixed. So, the cross section rotation is very sensitive to the span length (square function). For example, L_1=25ft, L_2=20ft, at the same midspan moment, Δ_1/Δ_2=1.5625, which means that the cross section of L_1 rotates approximately one and half times greater than the one of L_2.

Appendix E – Sample AISI Ballot

(14) The design yield stress of the member does not exceed 60 ksi (410 MPa or 4220 kg/cm2).

If variables fall outside any of the above stated limits, the user shall perform full-scale tests in accordance with Section F1 of this *Specification* or apply a *rational engineering analysis* procedure. For continuous purlin systems in which adjacent bay span lengths vary by more than 20 percent, the R values for the adjacent bays shall be taken from Table D6.1.1-1. The user shall be permitted to perform tests in accordance with Section F1 as an alternate to the procedure described in this section.

TABLE D6.1.1-1
Simple Span C- or Z-Section R Values

Depth Range, in. (mm)	Profile	R
d ≤ 6.5 (165)	C or Z	0.70
6.5 (165) < d ≤ 8.5 (216)	C or Z	0.65
8.5 (216) < d ≤ 11.5 (292)	Z	0.50
8.5 (216) < d ≤ 11.5 (292)	C	0.40

For simple span members, R shall be reduced for the effects of compressed insulation between the sheeting and the member. The reduction shall be calculated by multiplying R from Table D6.1.1-1 by the following correction factor, r:

$r = 1.00 - 0.01\ t_i$ when t_i is in inches (*Eq.* D6.1.1-2)

$r = 1.00 - 0.0004\ t_i$ when t_i is in millimeters (*Eq.* D6.1.1-3)

where

t_i = Thickness of uncompressed glass fiber blanket insulation

For simple span and continuous span members with rigid board insulation of thickness less than or equal to 4 in., R shall be 0.50 for Z-sections and 0.40 for C-sections for member depths less than or equal to 11.5 in. The rigid board insulation shall have a minimum compressive strength of 25 psi, and when using 4 in. of insulation, #14-1/4 fasteners or equivalent are required.

Form
0.19"
1.17

D6.1.2 Flexural Members Having One Flange Fastened to a Standing Seam Roof System

See Section D6.1.2 of Appendix A or B for the provisions of this section. A,B

D6.1.3 Compression Members Having One Flange Through-Fastened to Deck or Sheathing

These provisions shall apply to C- or Z-sections concentrically loaded along their longitudinal axis, with only one flange attached to deck or sheathing with through fasteners.

The nominal axial strength [resistance] of simple span or continuous C- or Z-sections shall be calculated in accordance with (a) and (b).

(a) The weak axis *nominal strength* [resistance] shall be calculated in accordance with Eq. D6.1.3-1. The *safety factor* and *resistance factors* given in this section shall be used to determine the allowable axial strength or design axial strength [factored compressive resistance] in accordance with the applicable design method in Section A4, A5, or A6.

revised to permit purlin systems with adjacent span lengths varying more than 20 percent to use the reduction factor, R, for the simply supported condition. The revision allows a row of continuous purlins to be treated with a continuous beam condition R-factor in some bays and a simple span beam condition R-factor in others. The 20 percent span variation rule is a local effect and as such, only variation in adjacent spans is relevant.

In 2011, R factors for through-fastened flexural members with rigid board insulation were added based on simple span girt tests by Gao and Moen (2011). For locally slender cross-sections, member local buckling and cross-section distortion dominated the failure mode. In this case the influence of insulation on capacity was minimal. For locally stocky cross-sections, the members rotated rigidly, causing prying action and a concentrated moment at the fastener connection that could not be efficiently resisted because of the insulation gap between member and sheeting. The concentrated moment resulted in bent and broken fasteners that compromised rotational restraint and reduced member capacity.

Although the tests focus on simple span girts, the experimentally derived R factors are applied to both simple and continuous spans with rigid board insulation. This assumption is justified by an analytical study in Gao and Moen (2011a) where cross-section prying action in the positive moment region of continuous spans is predicted to be consistent with or less than that observed in their simple span tests.

D6.1.2 Flexural Members Having One Flange Fastened to a Standing Seam Roof System

The design provision of this section is only applicable to the United States and Mexico. The discussion for this section is provided in the *Commentary* on Appendix A. 

D6.1.3 Compression Members Having One Flange Through-Fastened to Deck or Sheathing

For axially loaded C- or Z- sections having one flange attached to deck or sheathing and the other flange unbraced, e.g., a roof purlin or wall girt subjected to wind or seismic generated compression forces, the axial load capacity is less than a fully braced member, but greater than an unbraced member. The partial restraint relative to weak axis buckling is a function of the rotational stiffness provided by the panel-to-purlin connection. *Specification* Equation D6.1.3-1 is used to calculate the weak axis capacity. This equation is not valid for sections attached to standing seam roofs. The equation was developed by Glaser, Kaehler and Fisher (1994) and is also based on the work contained in the reports of Hatch, Easterling and Murray (1990) and Simaan (1973).

A limitation on the maximum yield stress of the C- or Z- section is not given in the *Specification* since *Specification* Equation D6.1.3-1 is based on elastic buckling criteria. A limitation on minimum length is not contained in the *Specification* because Equation D6.1.3-1 is conservative for spans less than 15 feet. The gross area, A, has been used rather than the effective area, A_e, because the ultimate axial stress is generally not large enough to result in a significant reduction in the effective area for common cross section geometries.

As indicated in the *Specification*, the strong axis axial load capacity is determined assuming that the weak axis of the strut is braced.

The controlling axial capacity (weak or strong axis) is suitable for usage in the combined axial load and bending equations in Section C5 of the *Specification* (Hatch, Easterling, and Murray, 1990).